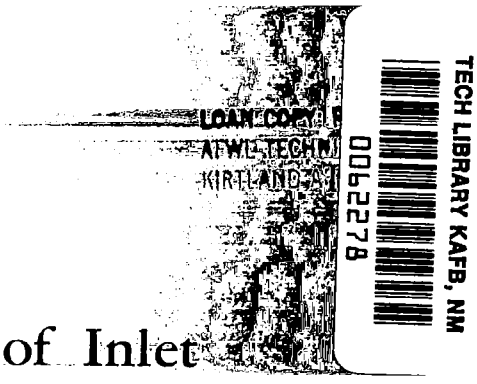

NASA Contractor Report 3416

Investigation of the Effects of Inlet Shapes on Fan Noise Radiation

T. L. Clark, D. R. Slotboom,
and P. G. Vaidya

CONTRACT NAS1-15394
APRIL 1981

NASA

NASA Contractor Report 3416

Investigation of the Effects of Inlet Shapes on Fan Noise Radiation

T. L. Clark, D. R. Slotboom,
and P. G. Vaidya
Boeing Commercial Airplane Company
Seattle, Washington

Prepared for
Langley Research Center
under Contract NAS1-15394

National Aeronautics
and Space Administration

**Scientific and Technical
Information Branch**

1981

CONTENTS

FIGURES

SYMBOLS

a	Duct radius
$\bar{a}$	Radius of inlet open area
A_{mn}	Acoustic mode amplitude
$\bar{A}_{mn}$	Modified acoustic mode amplitude
f	Theoretical directivity function
G	Green's function
J_m	mth order Bessel function
J_m'	Derivative of mth order Bessel function
k	Wave number
$\underset{\sim}{k}$	Wave number vector
k_{mn}	Axial wave number of mnth acoustic mode
m	Circumferential mode number
n	Radial mode number
n_s	Surface normal coordinate
$\underset{\sim}{r}$	Position vector (field)
$\underset{\sim}{r}_s$	Position vector (surface)
R	Radial distance
$\underset{\sim}{R}$	Radial distance vector
S	Surface area
S_I	Inlet surface
z	Coordinate
α	Canting angle
μ_{mn}	Hardwall duct eigenvalues, zeros of J_m'
ρ	Cylindrical radial coordinate
ρ_s	Cylindrical radial coordinate
ψ	Cylindrical or spherical polar angle coordinate
ψ_s	Cylindrical or spherical polar angle coordinate
ϕ	Velocity potential, right-going in duct
ϕ_I	Velocity potential, total in duct
ϕ_r	Velocity potential, left-going in duct
ϕ_E	Velocity potential, exterior to duct
θ	Spherical azimuthal angle (arc angle)
θ_s	Spherical azimuthal angle
$\bar{\theta}$	Spherical azimuthal angle (arc angle of peak SPL value)

1.0 SUMMARY

Some experiments were performed to gain an understanding of the effect the shape of an inlet has upon the directivity of radiated fan noise. The study was simplified to include only the zero flow condition. The previous works of references 1 and 2 demonstrated the existence of a shape effect in model fan testing but did not clarify the acoustic interactions that produced the effect. It was the intention of this study to remove the complexity of flow from the problem, to compare standard theoretical predictions with experiment for a full understanding of the simplest geometries and then to investigate experimentally and theoretically some less simple, nonstandard geometries for understanding the zero flow shape effect.

A vibrating plate mode generator produced a small set of acoustic modes in a circular duct that was connected to each of a number of zero flow inlets. The radiation directivity of each inlet for a given source condition was measured on the far field hemisphere by a microphone that traversed on a quarter circle arc for a series of duct rotation angles that covered an entire 360^0 rotation. It is shown that standard straight pipe radiation theories agree well with the data and that for well-cut-on modes, the radiation from a straight pipe inlet is not significantly affected by the presence of a baffle. The conical and exponential inlets display a tendency to focus the sound more forward compared to the straight pipe inlet while the toroidal inlet produces results that differ relatively little from the straight pipe inlet radiation patterns. An asymmetric straight pipe inlet produces an asymmetric three-dimensional radiation pattern that varies by as much as 18dB around the axis of the pipe.

2.0 INTRODUCTION

When sound at a single frequency is generated within an open ended duct, it will propagate through the duct and either radiate from the open end or be absorbed in the duct. On a far field sphere centered on the open end of the duct, a directivity pattern of the sound pressure level will form that is characteristic of: (1) the source of sound, or the duct acoustic modes that it excites; (2) the sound frequency; (3) the size and shape of the duct and the nature of its walls; (4) the steady state condition of the air column in the duct and in the air outside the duct, and finally; (5) the shape of the open end or termination or "inlet" of the duct and the nature of its wall material. It is well known that (1), (2), (3), and (4) are determining factors for the directivity pattern while the situation has not been so clear for (5). The uncertainty of the extent to which (5) influences the resulting directivity pattern is due more to a lack of information rather than conflicting sets of information. Only recently was it shown that the shape of the inlet indeed plays a significant role in the radiation of fan noise from inlets in static tests (refs. 1 and 2). Because the shape of the inlet determines the non-uniform steady state flow in the intermediate region between inside and outside the duct, there are two effects, normally confronted as separate effects, which are coupled to some unknown extent under the name of "inlet shape." These two effects are the strictly geometric boundary effect coming under classical diffraction theory and the non-uniform flow effect coming under classical refraction theory.

It was the objective of the present study to further investigate (5), but under the simpler conditions in which there is no mean airflow. The simplest imaginable situation would be to have a hardwall duct of circular cross section in which there is zero flow and only one acoustic mode at a single frequency propagating toward the open end of the duct, which is itself simply the cross section of the duct at which the duct ends – no shape change at all, only an abrupt end – with, possibly, a very large baffle or flange. There are well known solutions to this ideal problem (refs. 3, 4, 5, and 6) and the comparison of these with experimental data will give a kind of calibration to the expectations for less well developed solutions to geometrically more involved duct terminations. We fell short of the ideal situation experimentally only in that we always had more than a single acoustic mode. The resulting "calibration comparison" will be shown and discussed later in the results section of this report. The other duct terminations considered in this study were chosen either because of their geometrical and, therefore, analytical simplicity or because of the intrinsic interest of the data and the comparison it would provide for the simpler terminations. The conical and toroidal "inlets" are the first kind and the exponential and straight asymmetrical inlets are the second kind. The experimental hardware and procedures will be described in the next section. After this the experimental and theoretical results and comparisons will be presented.

The authors wish to acknowledge with appreciation the contributions to this work of A. O. Andersson, J. P. Roundhill, J. F. Newton, and D. Chestnutt.

3.0 EXPERIMENTS

3.1 INTRODUCTION

The experiments consisted of measuring in the far field a single frequency SPL over a circular arc (fig. 1) to determine the directivity of the sound radiated from each of a number of different duct open terminations, or inlets. The sound was generated in a long circular duct by a thin metal plate spanning a duct cross section in a plane perpendicular to the axis of the duct and thus forming a closed end for the air in the duct. This plate was made to vibrate at one of its resonant frequencies by electromagnetic drivers. At resonance the plate vibrates in a characteristic standing wave pattern which is communicated to the air in the duct. This plate-to-air coupling is not diagonal, or one-to-one, in the radial modes so that all the duct acoustic modes that are cut-on at the given frequency and having the same circumferential mode number as the plate mode will be excited. The source-duct-inlet assembly could be rotated on its axis so that the SPL on the complete far field hemisphere was measurable.

3.2 TEST ENVIRONMENT AND HARDWARE

All the tests were conducted in a large anechoic chamber of floor dimensions 22.86 x 19.81 m (75 ft x 65 ft) and height 10.67 m (35 ft). The walls, floor, and ceiling are covered with 0.41-m (16-in.) foam wedges and the dimensions above are from wedge tip to wedge tip. The axis of the duct assembly was half way between the floor and ceiling and 4.57 m (15 ft) from the nearest wall (wedge tip) and the plane of the open face of the duct termination (the inlet hilite plane) was located 4.57 m (15 ft) from the wall through which the duct assembly protruded.

The source-duct-inlet assembly consisted of three sections (fig. 2). The central section was a metal duct 0.914-m (3-ft) long with inner diameter of 0.298 m (11.75 in.) at one end of which was attached the vibrating plate mode generator. Another duct was attached to the rear of the mode generator to prohibit sound from radiating out the back directly into the room. All the inlets were then attached to the open, or front, end of the long duct.

Five different inlet sections were fabricated, each 0.61-m (2-ft) long from the plane of interface with the source duct to the extreme open end or hilite plane. Two of these were initially identical, simple circular ducts with an inner diameter equal to that of the source duct. These will be referred to hereafter as "straight pipe" inlets. One of these was ground down over a length of 0.0254 m (1 in.) on the outer wall to taper it down to the leading edge to a thickness of 0.1 times the original wall thickness, which was 0.00635 m (0.25 in.). The unmodified straight pipe inlet then became the "thick lip" inlet to distinguish it from the thin lip inlet (fig. 3).

The three other inlet sections were a conical section, a toroidal section, and an exponential surface of revolution section. Again, each of these was 0.61-m (2-ft) long. Also, each of these had the same open end diameters in the hilite plane, which was twice the diameter of the source duct. The conical inlet (fig. 4) had a cone angle of

26.57° (0.462 rad.) so that it consisted of a 0.305-m (1-ft) long section of circular duct and then a 0.305-m (1-ft) long section of a cone that expands from the original source duct diameter to twice this diameter.

The toroidal inlet (fig. 5) consisted of a 0.457-m (1.5-ft) long circular duct section joined smoothly to a half-torus. The radius of the torus, from duct axis to the center of the circle of revolution, is equal to one duct diameter and the diameter of the circle of revolution is equal to one duct diameter.

The exponential inlet (fig. 6) consisted of a 0.305-m (1-ft) long circular duct section joined smoothly (matched slopes) to an exponential surface of revolution, which was 0.305-m (1-ft) long and expanded from the duct diameter at the duct interface to twice the duct diameter at the hilite plane.

Two rings were fabricated (fig. 3), each 0.00635-m (0.25-in.) thick, both axially and radially. One of the rings fit flush inside the thick lip inlet and one fit flush outside the thick lip inlet. Two baffles (fig. 7) were fabricated to fit flush on the outside of the thick lip inlet. One baffle had an outer diameter of two duct diameters and one had an outer diameter of four duct diameters. One baffle was made for the conical inlet with an inner diameter twice a duct diameter and an outer diameter four times a duct diameter.

The three baffles, two rings, and five inlet sections make up 10 inlet configurations. An eleventh inlet was obtained by cutting the thick lip at an angle of 60° to the duct axis. This created what will be referred to as an asymmetric inlet.

The source-duct-inlet assembly was connected to a rotation mechanism (fig. 2) which held the assembly in place and provided for rotation of the assembly about its axis through a complete 360° rotation in discrete 5° increments.

The far field measurements were made with a single microphone attached to the top of a vertical pole (fig. 1) which was connected to a horizontal arm that was fixed at a point directly under the intersection of the inlet hilite plane and the duct axis. The pole-arm connection ran on wheels over a fixed circular track. This allowed the microphone to traverse a quarter circle arc of radius 4.57 m (15 ft) in a plane containing the duct axis. The arc was oriented so that 0° was along the duct axis and 90° was perpendicular to the duct axis. Measurements were made at the traverse angular speed of 2 deg/sec and since the averaging time to produce an SPL value was well under a second, the angular resolution possible with this system was at least 2°. That is to say, the angular information from the continuous traverse should be at least as detailed as having stationary microphones placed on the arc at 2° intervals. By alternating between duct rotation and microphone traverse, the complete forward hemisphere radiation directivity of any of the source-inlet combinations could be measured.

3.3 DATA ACQUISITION AND ANALYSIS

The single frequency SPL data from the traversing microphone together with the traverse position data and the duct rotation angle were the main data acquired during each test. In addition to these, the single frequency SPL data from a stationary

microphone was acquired to provide a check on the constancy of the source during each test, and voltage "pips" indicating the coincidence of the traversing microphone with the 0^0 and the 90^0 positions were acquired. A test, or test run, took about 45 sec to complete and all acquired data were FM recorded on analog magnetic tape at 60 IPS. The traversing microphone SPL and position data were also displayed on an X-Y plotter online during each test run.

The analog data was digitized at the rate of 10 samples/sec and then averaged to produce 91 pairs of data points per test run for the traversing microphone SPL and position (0^0 to 90^0). Although it was ascertained before and during the test that the microphone pole traversed the arc at a sufficiently constant speed that the angular resolution of 2^0 was maintained, the digitized position data showed considerable variability. The analog position data were generated as the DC voltage of a potentiometer and it was determined that the FM taping and the analog-to-digital conversion together introduced sufficient noise to this data to account for the variability. To smooth the digital microphone position data, a straight line was least squares fitted to the position versus time plot of the data. The final 91 position values were extracted from this straight line.

The first phase of the experiments consisted in establishing the relevant noise floors and reducing them where needed. The two possible noise floors of concern were first the combined ambient plus traversing microphone system noise and second the noise from the vibrating plate that arrived at the microphone position by any path other than direct radiation from the open end of the inlets. The first type of noise was shown to be broadband and to contribute no more than 25 dB in the frequency bands of interest. Since the direct radiation sound pressure levels had maximum values of 80 dB, this first noise floor would limit the angular dynamic range to 55 dB.

However, the second noise floor was determined to be even higher, about 40 dB at all far field microphone positions, and it was this indirect radiation from the duct and inlet walls that limited the range of a lobe in a measured directivity pattern to 35 dB to 40 dB (minimum to maximum).

The vibrating plate mode generator is described in reference 7. The plate has many resonant vibration frequencies in the range from around 2 to 20 KHz. These frequencies are fixed for all practical purposes and at each frequency the plate vibrates in a single mode specified by a circumferential mode number and a radial mode eigenvalue. To achieve a spinning, or circumferentially traveling, plate mode rather than a standing wave plate mode, two external magnetic drivers were applied to the plate. These drivers were circumferentially 90^0 apart and operated at a quarter of a cycle out of phase. The radial location of the drivers was determined by the maximum of the radial vibration eigenfunction. Spinning plate modes of odd circumferential mode numbers could thus be generated. In practice, for the three resonant frequencies used in these experiments, a residual standing wave component remained due to incomplete cancellation from the two drivers. Sufficient cancellation did take place to keep the "ripple" in the circumferential direction in the far field SPL to less than 3 dB (requiring an amplitude difference of at least 6 to 1).

The radial eigenfunction for the plate vibration is not equal to any of the duct acoustic radial eigenfunctions for the same circumferential mode number. Thus all the duct acoustic modes up to cut-off with the circumferential mode number the same as the plate circumferential mode number will be excited. There were three plate resonances chosen for these experiments (table 1). Two of these had a circumferential mode number, m = 13, and one had m = 11. The lowest frequency plate resonance was 7.996 KHz and corresponded to the plate vibration mode m =13 and n = 1, or the (13,1) plate mode (n is the radial eigenvalue index and has the possible values n = 1, 2, 3, . . .). The second resonance was at the frequency of 11.971 KHz with the plate mode (13,2) and the third resonance was at the frequency 13.471 KHz with the plate mode (11,3). The acoustic nondimensional wave numbers, or ka values, for these three frequencies are, respectively, 21.58, 32.30, and 36.20. The correspondingly nondimensionalized acoustic radial eigenvalues for a hardwall circular duct and m = 13 are: n = 1, 14.93, n = 2, 19.88; n = 3, 23.82; n = 4, 27.47; n = 5, 30.99; n = 6, 34.41. For m = 11, they go from n = 1, 12.83 to n = 7, 35.17 and n = 8, 38.46, covering our range of interest. Thus the (13,1) plate mode gives rise to the first two duct acoustic modes for m = 13; the (13,2) plate mode gives rise to the first five duct acoustic modes for m = 13; and the (11,3) plate mode gives rise to the first seven duct acoustic modes for m = 11. Figures 8a and 8b display, for m = 11 and 13, estimates of the relative amplitudes of the different duct acoustic modes assuming a simple unloaded plate model for the coupling of the plate vibration to the air column in the duct (ref. 7).

4.0 RESULTS

4.1 THEORETICAL CONSIDERATIONS

The theory and mathematical analysis of acoustic radiation from what are referred to in this report as straight pipe inlets have been well developed and documented (refs. 3, 4, 5, and 6). These theories have been used, in one form or another, by most researchers who predict the radiation of fan tone noise from inlets. References 8 and 9, in particular, used the baffled straight pipe inlet analysis in their work and reference 10 adapted for fan noise prediction the analysis of the unbaffled straight pipe inlet. The only reason one considers the use of baffles in the context of fan noise radiation from inlets, of course, is the mathematical simplification involved. This simplification results relative to the unbaffled straight pipe mathematics, however, only so long as the reflection of sound waves from the duct open end back into the duct can be neglected. Thus the advantage disappears in those situations, for instance, where modes are just cut-on. Except for these situations, the baffled and unbaffled analyses yield virtually identical results. To use simplified baffled inlet analysis for fan noise prediction it must be assumed that not only is reflection from the open end negligible but that the variation of the inlet shape from that of a straight pipe has negligible effect. It has yet to be determined for practical inlets that are used in static tests and in flight conditions the extent to which these assumptions are generally valid.

The mathematical formulations of the radiation problem derive from the Helmholtz equation and the hardwall boundary condition for a linear field variable such as the velocity potential. In particular, the integral equation formulations follow upon the introduction of the Green's function for the Helmholtz equation (ref. 3, Chapter 7). Green's integral theorem provides for combining the differential equation and boundary conditions into an integral equation. The application of this theorem requires the choice of a boundary surface and two such surfaces suggest themselves in the problem of radiation from inlet openings. These surfaces are illustrated in figures 9a and 9b. For straight pipe inlets, the choice of surface in figure 9a leads to the Levine-Schwinger and Weinstein formulation which Lansing (ref. 10), after generalizing to include uniform flow, applied to the fan noise prediction problem. A further distortion of the boundary surface of figure 9b leads to figure 9c and then the introduction of a hardwall baffle on this new surface gives figure 9d. The resulting simplicity follows immediately from requiring that the Green's function, as well as the velocity potential, satisfies the hardwall boundary condition on the baffle. That is, add to the simple Green's function its mirror image in the baffle. Assuming the velocity potential satisfies the radiation condition, the representation of the potential anywhere in the exterior space of figure 9d in terms of its surface values and normal derivatives, required by Green's theorem, is simply

$$\phi_E(\underset{\sim}{r}) = \iint_{S_I} G(\underset{\sim}{r}|\underset{\sim}{r}_s) \frac{\partial \phi_E(\underset{\sim}{r}_s)}{\partial n_s} ds \qquad (1)$$

where G is the appropriate Green s function, $\partial\phi_E/\partial n_s$ is the outward normal derivative and S_I is the open area of the inlet in the plane of the baffle. If the potential in the

interior region is given by a sum of right-going (ϕ_i) and left-going (ϕ_r) waves, then $\phi_I=\phi_i+\phi_r$. When ϕ_E and ϕ_I and their normal derivatives (particle velocities) are matched on their common boundary, S_I, then an integral equation results coupling ϕ_i and ϕ_r and the representation of the exterior potential becomes

$$\phi_E(\underset{\sim}{r}) = \iint_{S_I} G(\underset{\sim}{r}|\underset{\sim}{r}_s) \frac{\partial \phi_I(\underset{\sim}{r}_s)}{\partial n_s} ds \tag{2}$$

If ϕ_i is known, corresponding to a semi-infinite interior region, or if both ϕ_i and ϕ_r are coupled at another interior surface where a known vibration occurs, etc., then ϕ_i can be considered known when the integral equation representing the coupling at the inlet open end is solved. The interior potentials are generally represented by a normal mode expansion with propagation or decay in the axial direction. It has been shown that for the symmetric semi-infinite straight pipe inlet with baffle, when ϕ_i is a single mode just cut-on, then ϕ_r is significant and comparable to ϕ_i in magnitude. However, when ϕ_i is a single mode that is well-cut-on, ϕ_r is insignificant compared to ϕ_i in magnitude.

In this case, for well-cut-on modes, the representation for the exterior potential becomes

$$\phi_E(\underset{\sim}{r}) \simeq \iint_{S_I} G(\underset{\sim}{r}|\underset{\sim}{r}_s) \frac{\partial \phi_i(\underset{\sim}{r}_s)}{\partial n_s} ds \tag{3}$$

Since the experimental data is for the most part in the well-cut-on mode range, we will restrict the theoretical considerations to this case. Thus it is assumed for the comparisons to be made in this report that modal reflections and cross-coupling at the inlet open ends will be negligible. Baffled inlet models then can use equation (3) with G replaced by its asymptotic form (see fig. 10)

$$G(\underset{\sim}{r}|\underset{\sim}{r}_s) \simeq \frac{e^{ikR}}{2\pi R} e^{-i\underset{\sim}{k}\cdot\underset{\sim}{r}_s} \tag{4}$$

to compute the far field solution for the potential. Here

$$\underset{\sim}{k} = \underset{\sim}{k}R/R \tag{5}$$

and (see fig. 11)

$$\underset{\sim}{k}\cdot\underset{\sim}{r}_s = kr_s(\cos\theta\cos\theta_s + \cos(\psi - \psi_s)\sin\theta\sin\theta_s) \tag{6}$$

The common form of representing this solution is as a diverging spherical wave with a directivity function multiplying the point source wave function

$$\phi_E(\underset{\sim}{r}) \simeq f(\theta,\psi)\,\frac{e^{ikR}}{4\pi R} \tag{7}$$

where

$$f(\theta,\psi) = 2\iint_{S_I} \frac{\partial\phi_i(\underset{\sim}{r}_s)}{\partial n_s}\, e^{-i\underset{\sim}{k}\cdot\underset{\sim}{r}_s}\, ds \tag{8}$$

When a single acoustic mode is excited in the circular duct, it will be represented by the mode function

$$\phi_i = A_{mn}\, J_m\,(\mu_{mn}\rho/a)\, e^{im\psi}\, e^{ik_{mn}z} \tag{9}$$

where A_{mn} is the mode amplitude, $J_m(x)$ is the mth order Bessel function, μ_{mn} is the nth zero of the derivative of the Bessel function and

$$k_{mn} = \sqrt{k^2a^2 - \mu_{mn}^2}\Big/a \tag{10}$$

For the simplest case of the straight pipe (symmetrical) inlet with the open end and the baffle in the z = 0 plane, $\theta_s = \pi/2$ and equation (8) gives

$$f(\theta,\psi) = -2i\, A_{mn}\, k_{mn} \int_0^a J_m\,(\mu_{mn}\rho_s/a) \int_0^{2\pi} e^{im\psi_s}\, e^{-ik\rho_s \sin\theta\cos(\psi-\psi_s)}\, d\psi_s \rho_s d\rho_s$$

$$= 2(-i)^{m+1}\, A_{mn}\, k_{mn} a^2\, \frac{ka\,\sin\theta J_m'(ka\sin\theta)\, J_m\,(\mu_{mn})}{\mu_{mn}^2 - k^2a^2\sin^2\theta}\, e^{im\psi} \tag{11}$$

To utilize equation (8) for the more general symmetric inlets, a way must be found to compute $\partial\phi_i/\partial z$ on S_I knowing ϕ_i in the circular duct. The problem is essentially that of propagation in a variable area duct which is a difficult problem on its own and outside the scope of this report. However, if the simplest assumptions are made regarding this transmission problem then the very crudest approximation to $\partial\phi_i/\partial z$ on S_I can be made and, thus, to $f(\theta,\psi)$ also. If, then, ϕ_i near S_I can be approximated by a single circular duct hardwall mode function for a duct with radius equal to the radius of the hilite point of the inlet face with mode amplitude determined by the mode amplitude of the original mode in the circular duct through an energy conservation criterion, and the mode numbers are the same as for the original mode, this results in $f(\theta,\psi)$ having the same expression as in equation (11) with a different mode amplitude and a new radius, say $\bar{A}_{mn}$ and $\bar{a}$, so that

$$f(\theta, \psi) \simeq 2(-i)^{m+1} \bar{A}_{mn} k_{mn} \bar{a}^2 \frac{k\bar{a} J_m'(k\bar{a} \sin\theta)\, J_m(\mu_{mn})}{\mu_{mn}^2 - k^2\bar{a}^2 \sin^2\theta} e^{im\psi} \tag{12}$$

The dominant lobe for the directivity pattern of the straight pipe inlet is centered very nearly on the azimuthal angle θ given by

$$\sin\theta = \mu_{mn}/ka \tag{13}$$

The corresponding prediction of this crude model for the nonstraight pipe inlets is $\bar{\theta}$, say, where

$$\sin\bar{\theta} \approx \frac{a}{\bar{a}} \sin\theta \tag{14}$$

As will be shown in the data comparisons, this prediction is actually fairly accurate for the cone inlet, slightly less so for the exponential inlet and completely misleading for the toroidal inlet. Of course, at this level, this model cannot account for any shape effects at all. These effects would enter in the next level of approximation in this model when the contoured inlet walls are considered in the variable area duct transmission problem.

There are several alternatives to this type of modeling for symmetric, nonstraight pipe inlets. One of these is actually a duct transmission problem where the inlet walls are allowed to diverge to infinity. Far from the circular duct and inlet interface and not too close to the expanding inlet walls, the acoustic field is an expanding wave front with an inlet shape effect coming mainly from the area around the duct-inlet interface. An example of this approach is given in references 11 and 12 in which the "inlet" walls are an hyperboloid of revolution. A second alternative is a strictly numerical solution to the well-posed integral equation formulation (without a baffle) of the radiation problem. References 13 and 14 exemplify this approach and show that continuing research in this area does indeed show promise for the future. A third alternative in which are sought approximate analytical and numerical solutions to an integral equation formulation of the (unbaffled) symmetric inlet radiation problem shows promise also, but has yet to produce significant results.

The theory that is compared with the unbaffled straight pipe inlet experimental data is essentially that of references 5 and 6 and, therefore, of reference 10 with zero mean flow.

The only asymmetric inlet studied in this work was the straight pipe inlet whose open end is in the plane cutting the duct axis at an acute angle (experimentally = 60^0). The boundary of the inlet open area in this plane is then an ellipse and the normal to this area forms an acute angle (experimentally = 30^0) with the duct axis. Assuming that the presence of a baffle in the plane of the inlet open area will not significantly affect the far field directivity function for well-cut-on modes in the circular duct, then equation (8) can be used to compute this directivity. To use this formulation directly, however, requires that the exterior coordinate system be defined by the plane of the baffle being

the z = 0 plane, with the z-axis given by the line normal to this plane and intersecting the center of the open area of the inlet. The normal derivative of the velocity potential on the inlet open area in this case has three terms

$$\frac{\partial \phi_i}{\partial n_s} = -\cos\alpha \frac{\partial \phi_i}{\partial z_s} - \sin\alpha \sin\psi_s \frac{\partial \phi_i}{\partial \rho_s} - \sin\alpha \cos\psi_s \frac{1}{\rho_s} \frac{\partial \phi_i}{\partial \psi_s} \tag{15}$$

When α goes to zero, only the first term remains and the symmetric baffled inlet condition is regained. For general non-zero α, this result for $\partial\phi_i/\partial n_s$ produces three terms in the expression for f (θ,ψ) in equation (8). Each of these terms is an area integral which can be converted to an infinite sum of single integrals and, thence, approximately to a single integral which must be evaluated numerically (except for the first of the three terms which can be evaluated analytically, as in the symmetric inlet case). A more complete discussion of this evaluation is presented in reference 15. The results of this analysis compare fairly well with the data (Section 4.4). Figure 12 is a prediction from this analysis of the change in peak level in the directivity pattern with canting angle (negative values for α indicate the far field arc on which the directivity pattern is considered is shown in the figure). It can be seen from this figure that canting affects the higher order modes more than the lower order modes. It can be speculated that since these modes are closer to cut-on and propagate at larger angles to the duct axes, they are more sensitive to the changing wall boundary conditions presented to them by the canted inlet.

4.2 STRAIGHT PIPE INLETS

Six variations of a straight pipe inlet were tested for three different plate vibration resonances. Figure 13 is a composite of the experimental directivities for the six inlet variations for the (11,3) plate mode. From 0^0 to 15^0 the data are around 40 dB and quite different from configuration to configuration. This region is dominated by indirect radiation and since the radiation is single frequency, complex interference effects can account for the configuration to configuration variability. From 15^0 to 90^0 the direct radiation from the open end of the inlets is dominant and a characteristic pattern of radiation emerges and is repeated with each inlet variation. If only one duct acoustic mode were generated by the plate and no significant mode cross-coupling took place at the inlet open end, then one would have expected a directivity pattern with a lobe number equal to the number of radial modes that satisfy the cut-on criterion for the given frequency and circumferential mode number. In this case that number is seven. That there are six lobes in the experimental directivity pattern is a result of there being many radial modes generated by the vibrating plate rather than just one. Even when the relative magnitudes of the mode amplitudes in the duct are fixed, varying the relative phases of the mode amplitudes will cause some variation in the directivity pattern. Figures 14a and 14b show the comparisons between theory and experiment that can be made when the relative magnitude of the mode amplitudes are assumed given by figure 8a. Using the plate mode n = 3 curve in this figure gives the 4th radial acoustic mode as the dominant one, the 1st, 2nd, 3rd, and 5th as reduced but significant and the

6th and 7th as rather less significant. The dominant lobe at about 43° is due mainly to the main lobe of the directivity pattern that the 4th radial mode alone would create. The absolute levels for the theoretical curves were not determined from theory but have been adjusted to coincide with the data near the peak levels. The relative phases between the acoustic modes have been chosen arbitrarily for these comparisons and it should be kept in mind that these phases can alter the results somewhat, although not so much as would be the case if the relative magnitudes of the mode amplitudes were more nearly equal.

It is apparent in figure 13 that some of the directivity patterns are shifted a constant 1° or 2° relative to the others. This is within the angular resolution of 2° that the data acquisition was designed for and resulted, it is thought, from the slight offset in alignment of the duct inlet assembly with the far field measuring arc. The duct-inlet assembly was withdrawn from the anechoic room for each inlet change and then reinserted and realigned. Other than this accountable difference there is little significant difference between the directivity patterns. The first four lobes, between 20° and 60°, are essentially identical for all the patterns. The lobe centered around 65° is 15 dB or more down from the main lobe and the sixth lobe (not even a distinct lobe for the short baffle inlet) is down at least 20 dB (except for the large baffle inlet where it is only 15 dB down). This outer or sideline region of the arc is different from the inner region in that the higher order radial modes, which have their dominant lobes in this region, have relatively insignificant power. Thus the directivity pattern at these angles is the result not of a few competing dominant lobes but of many competing dominant and secondary lobes. Relative phase differences between the duct modes are thus likely to be more significant for the directivity pattern in these outer angles. Small changes in the "edge condition" of the straight pipe inlet might then be expected to show up in changes in the outer region of the directivity pattern. Thus the experimental data are consistent with the theories for "well-cut-on" modes. As a calibration comparison, figures 14a and 14b indicate that the experimental data for the other, nonstraight or asymmetric, inlets should indeed provide a good test for the theories of the corresponding inlet shapes for well-cut-on modes.

Figure 15 is a composite of four experimental directivities for the (13,2) plate mode. The four inlets are the thick lip inlet, the thick lip with inner ring and the thick lip with the small and the large baffle. Here the number of propagating modes generated by the vibrating plate is five and there are five lobes in the directivity patterns. The minimum between the second and third lobes (at 42°) is hardly sufficient to define two lobes for the straight pipe inlet but with the slightest perturbation such as adding the thin inner ring to the open edge the minimum is deepened significantly. This angle coincides with the angle at which the dominant lobes of the 2nd and 3rd theoretical mode directivity patterns are of equal strength (see fig. 16a which is based on the results from fig. 8b). Thus the more these two modes are out of phase the deeper will be the minimum, and the notable difference in the experimental depth is due to slight relative phase changes accomplished during the radiation process and not due to a significant change in mode directivity patterns. Figure 16b is a comparison of the baffled inlet data with the theoretical directivity pattern for the third mode alone.

Figure 17a is a comparison of the unbaffled (thick lip) straight pipe experimental directivity pattern with a theoretical prediction using all five propagating modes weighted according to the results of figure 8b but given arbitrary relative phases. Figure 17b is a similar comparison for the large baffle-inlet case.

Figure 18 is a composite of two experimental directivities for the (13,1) plate mode. These are the thick lip and the large baffle inlets, respectively. They are seen to be essentially identical but for a 10^0 interval between 75^0 and 85^0. There are only two propagating modes in this case and the results from figure 8b are that the second mode, the one nearest cut-on, is stronger than the first mode. The single broad lobe in the experimental data is again due to the superposition of two directivity patterns, each of which has two lobes. Figure 19a shows the two theoretical directivity patterns for the two modes separately (with relative amplitudes from fig. 8b), for the unbaffled inlet, while figures 19b and 19c show the comparisons with the unbaffled and baffled inlet data and corresponding theoretical predictions, combining the two propagating modes, respectively. Based on these comparisons, one can expect the data for the remaining inlets to provide a limited but accurate experimental check on a theoretical prediction for any of these inlets.

4.3 SYMMETRIC INLETS

The data for these inlets is presented in figures 20, 21, and 22. The data for the thick lip straight pipe inlet is included as a baseline reference. In figure 20 the source is the (11,3) plate mode, in figure 21 the source is the (13,2) plate mode, and in figure 22 the source is the (13,1) plate mode. In the first two figures, the directivity patterns for the cone with and without a baffle are identical to within the experimental accuracy, while in the third figure a measurable difference appears. The (13,1) plate mode produces but two propagating acoustic modes in the duct. There was a small difference between the baffled and unbaffled straight pipe patterns as well (fig. 18). These observed differences can be due either to the effect of the baffle on the individual mode directivity patterns, expected for near cut-on modes, or to extra relative phase shifting of one of the modes on radiation with a baffle. In any case the first two source conditions give a strong indication that even for nonstraight pipe symmetric inlets, a baffle does not affect significantly the radiation characteristics of the original unbaffled inlet for well-cut-on modes.

Clearly the peak levels in the patterns of the cone and exponential inlets have shifted away from the sideline and toward the duct-inlet axis while the peak levels for the toroidal inlet are within a few degrees of the peak levels of the baseline inlet. The predicted angular shift of the peak levels from their position in the baseline inlet from equation (14) is for the (11,3) plate mode $43^0 \rightarrow 20^0$; for the (13,2) plate mode $47^0 \rightarrow 21.5^0$; and for the (13,1) plate mode $58^0 \rightarrow 25^0$. Although this might be said to give a reasonable prediction for the two well-cut-on mode source conditions for the cone inlet, the situation is in fact too complicated for this model to add much insight. The cone inlet patterns for these conditions have two equal peaks, if you will, at different angles, and the baseline patterns have but one peak. The exponential inlet has peaks in the vicinity of these predictions, also. The general prediction that the radiated sound power is "focused" more forward by the cone and exponential inlets is abundantly

confirmed by all three source conditions. This prediction is completely wrong when applied to the toroidal inlet for all three source conditions. This difference of the toroidal inlet from the other two may not be due to the geometrical shape so much, however, as simply the fact that the opening occurred more "abruptly," over a shorter distance, and therefore "looked" more like a straight pipe inlet. Such qualitative speculation, however, is no substitute for the clear insight provided by quantitative calculation. This is especially true when there is so little experimental data from which to form such speculations. These data show that there are inlet shape effects and provide a limited but accurate base for comparison with theory but are insufficient in themselves to classify or categorize these effects.

4.4 THE ASYMMETRIC INLET

The asymmetric inlet produces a directivity pattern on the far field arc that varies with the duct rotation angle. The test included gathering 65 directivity patterns for the three source conditions. The plane that includes the duct axis and cuts the inlet into two equal halves; i.e., contains the major axis of the ellipse bounding the open end of the inlet, is a plane of symmetry so that only one half of a full duct rotation need be considered. The test included gathering data over the full duct rotation and confirming the symmetry. The duct rotation angle of 90^0 is defined as the angle at which the plane of symmetry is normal to the plane of the measuring arc and 0^0 is the angle at which these two planes coincide and the normal to the open area of the inlet points toward the measuring arc. Figures 23, 24, and 25 are the directivity plots at the duct rotation angles of 0^0, 90^0, and 180^0 for the (11,3), (13,2), and (13,1) plate mode conditions, respectively. The directivity patterns at the 90^0 rotation angle are essentially the same as the baseline directivities, while the patterns at the 0^0 and the 180^0 rotation angles are quite different from the baseline. Figure 26 is a plot of the SPL at the arc angle of 45^0 versus the duct rotation angle for the (11,3) plate mode source condition. Figure 27 shows the comparison between the theory of reference 15 and the experimental results for four duct rotation angles.

5.0 CONCLUSIONS

The experimental results from this study support the following major conclusions:

1. The standard theories were shown to predict within experimental accuracy the radiation from baffled and unbaffled symmetric straight pipe inlets;

2. For the radiation of well-cut-on modes, adding a baffle or making small modifications to the edge of a straight pipe inlet did not change the radiation directivity to a significant degree;

3. The conical and exponential inlets focused the sound more forward relative to the straight pipe inlet radiation and it was shown that this is consistent with a simple estimate based solely on the increased open area of the inlets;

4. The toroidal inlet produced directivity patterns that differed in detail from the straight pipe inlet patterns but generally agreed with them more closely than the patterns produced by the conical and exponential inlets. This might be due to the greater curvature involved in this inlet compared to the other two symmetric contoured inlets;

5. The asymmetric straight pipe inlet produced directivity patterns that varied with the cylindrical polar angle (or duct rotation angle) with maxima and minima at the expected polar angles. An approximate analysis compared reasonably well with this data.

The small set of data encompassed by this study cannot support more general or practical conclusions without more detailed theoretical analyses of the different inlet shapes.

REFERENCES

1. Sloan, D., Rayl, C., and Farquhar, B. W.: "Investigation of Directional Inlets Utilizing Refraction," NASA CR 145210, March 1977.

2. Abbott, J. M.: "Aeroacoustic Performance of a Scoop Inlet," AIAA Paper No. 77-1354, AIAA 4th Aeroacoustics Conference, Atlanta, Georgia, October 1977.

3. Morse, P. M. and Feshbach, H.: *Methods of Theoretical Physics,* McGraw-Hill Book Company, Inc., New York, 1953.

4. Miles, J. W.: "The Coupling of a Cylindrical Tube to a Half-Infinite Space," Journal Acous. Soc. Am., Vol. 20, No. 5, 652, September 1948.

5. Levine, H. and Schwinger, J.: "On the Radiation of Sound From an Unflanged Circular Pipe," Phys. Rev., Vol. 73, No. 4, 383, February 1948.

6. Weinstein, L. A.: *The Theory of Diffraction and the Factorization Method (Generalized Weiner-Hopf Technique,* The Golden Press, Boulder, Colorado, 1969.

7. Joppa, P. D.: "Vibrating Plate Acoustic Mode Generator," Boeing Technical Document D6-48068, December 1979.

8. Tyler, J. M. and Sofrin, T. G.: "Axial Flow Noise Studies," SAE Trans. Vol. 70, 309, 1962.

9. Slutsky, S.: "Discrete Noise Generation and Propagation by a Fan Engine," AFOSR-UTIS Symposium on Aerodynamic Noise, Toronto, 1968.

10. Lansing, D. L.: "Exact Solution for Radiation of Sound From a Semi-Infinite Duct With Application to Fan and Compressor Noise," Symposium on Analytical Methods in Aircraft Aerodynamics, NASA SP-288, October 1969.

11. Cho, Y. C.: "Sound Radiation From Hyperboloidal Inlets Ducts," AIAA Paper No. 79-0677, March 1979.

12. Clark, L. R. and Cho, Y.C.: "An Experimental Study of Sound Radiation From Hyperboloidal Inlet Ducts," NASA Technical Memo 80109, June 1979.

13. Meyer, W. L., Bell, W. A., Stallybrass, M. P., and Zinn, B. T.: "Prediction of the Sound Field Radiated From Axisymmetric Surfaces," J. Acoust. Soc. Am. 65(3), 631, March 1979.

14. Meyer W. L., Bell, W. A. and Zinn, B. T.: "Prediction of the Sound Field Radiated From Axisymmetric Surfaces," AIAA Paper No. 78-195, January 1978.

15. Vaidya, P. G. and Slotboom, D.: "The Radiation Pattern of Asymmetric Inlets," AIAA Paper No. 80-0967, June 1980.

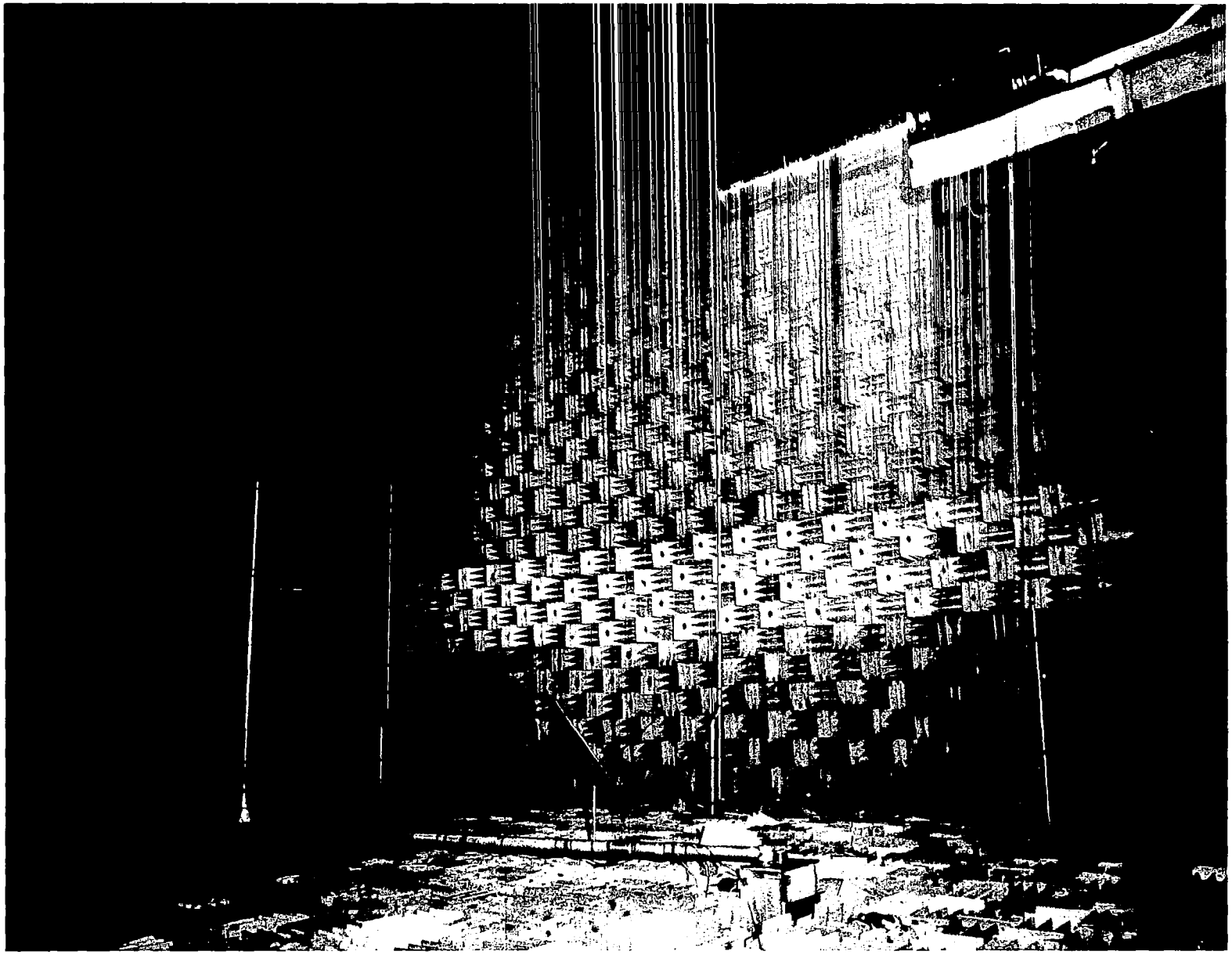

Figure 1. – Test Environment and Traversing Microphone

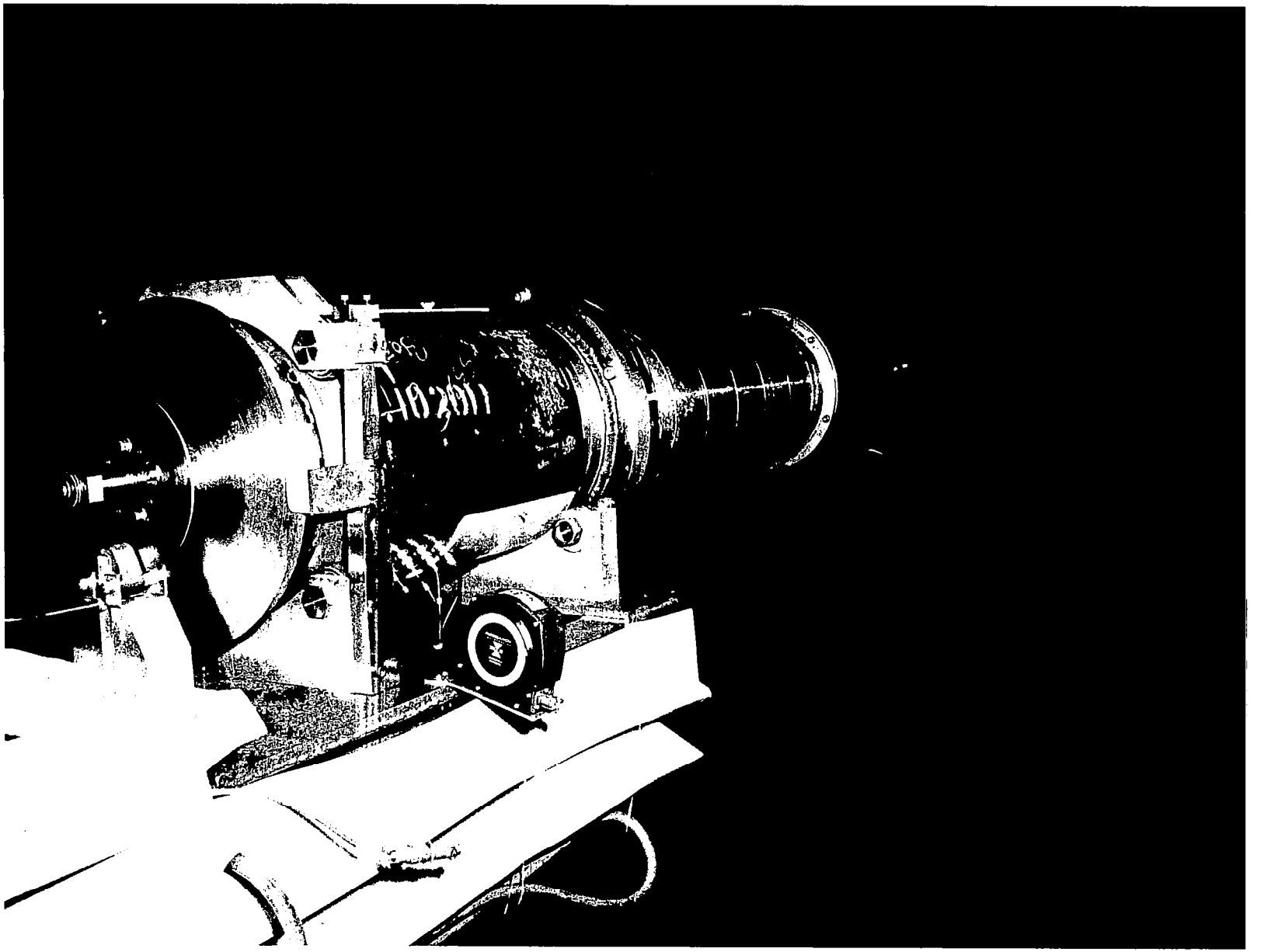

Figure 2. – Inlet-Duct-Source Assembly

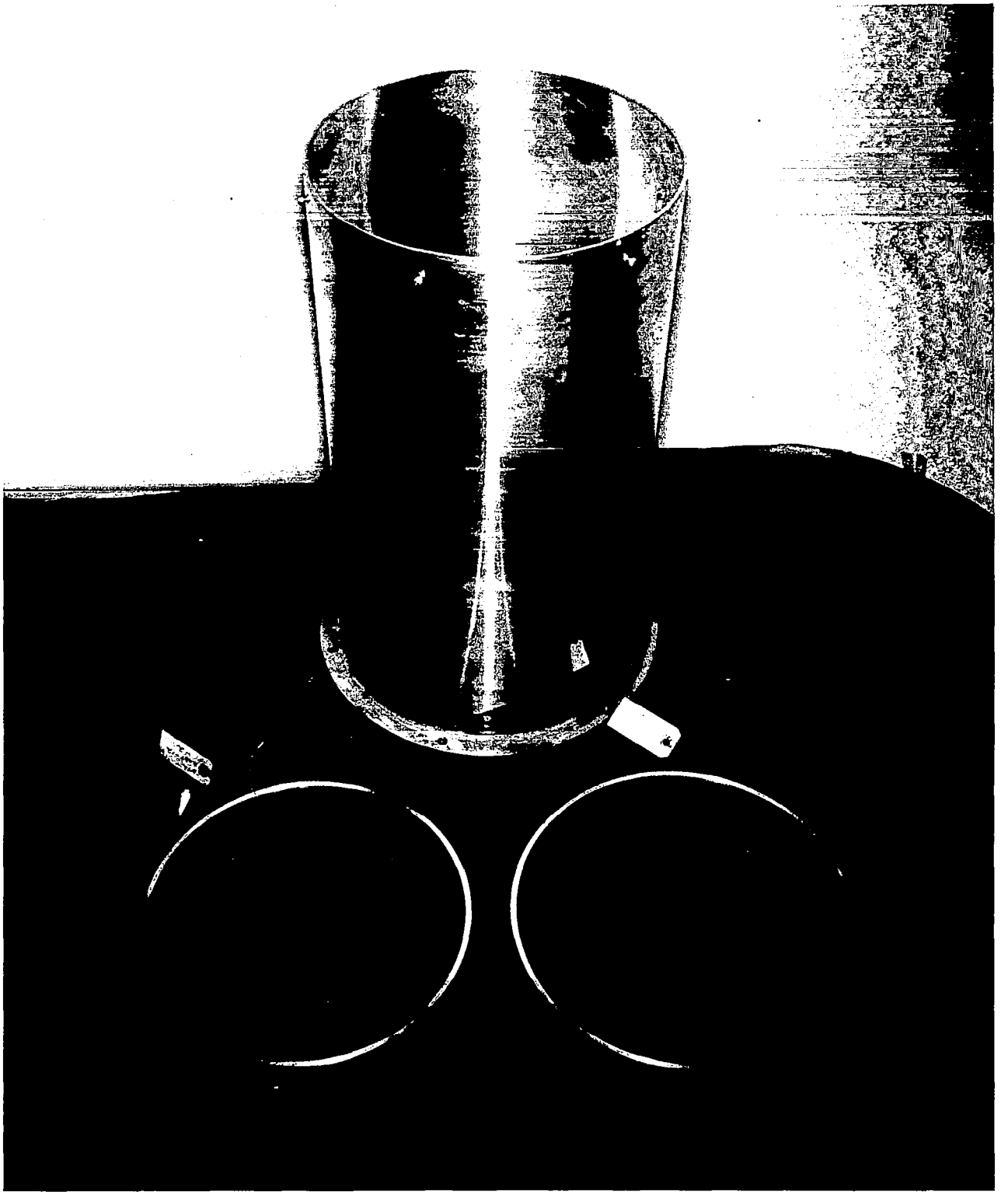

Figure 3. – Straight Pipe Inlet with Rings

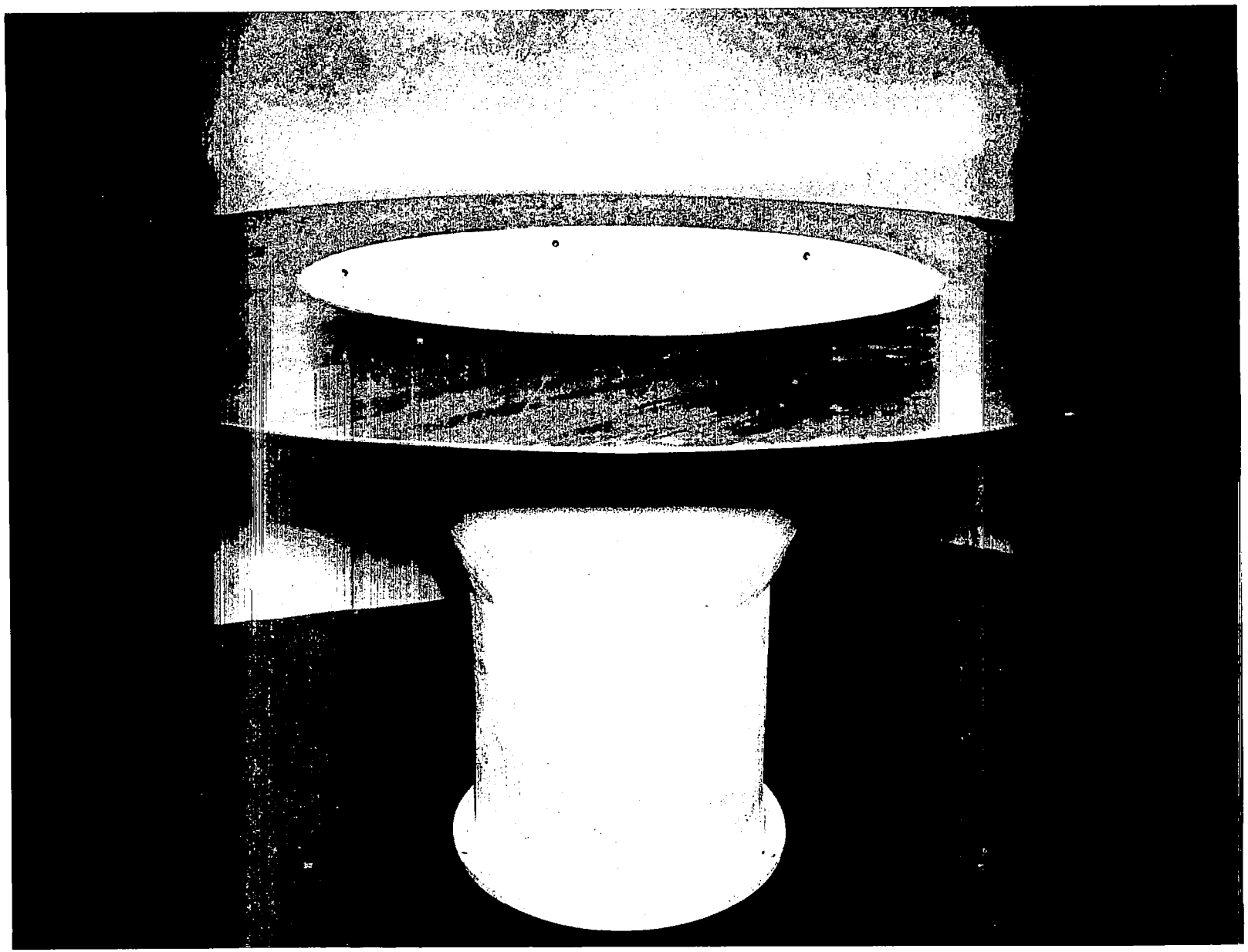

Figure 4. – Conical Inlet with Baffle

Figure 5. – Toroidal Inlet

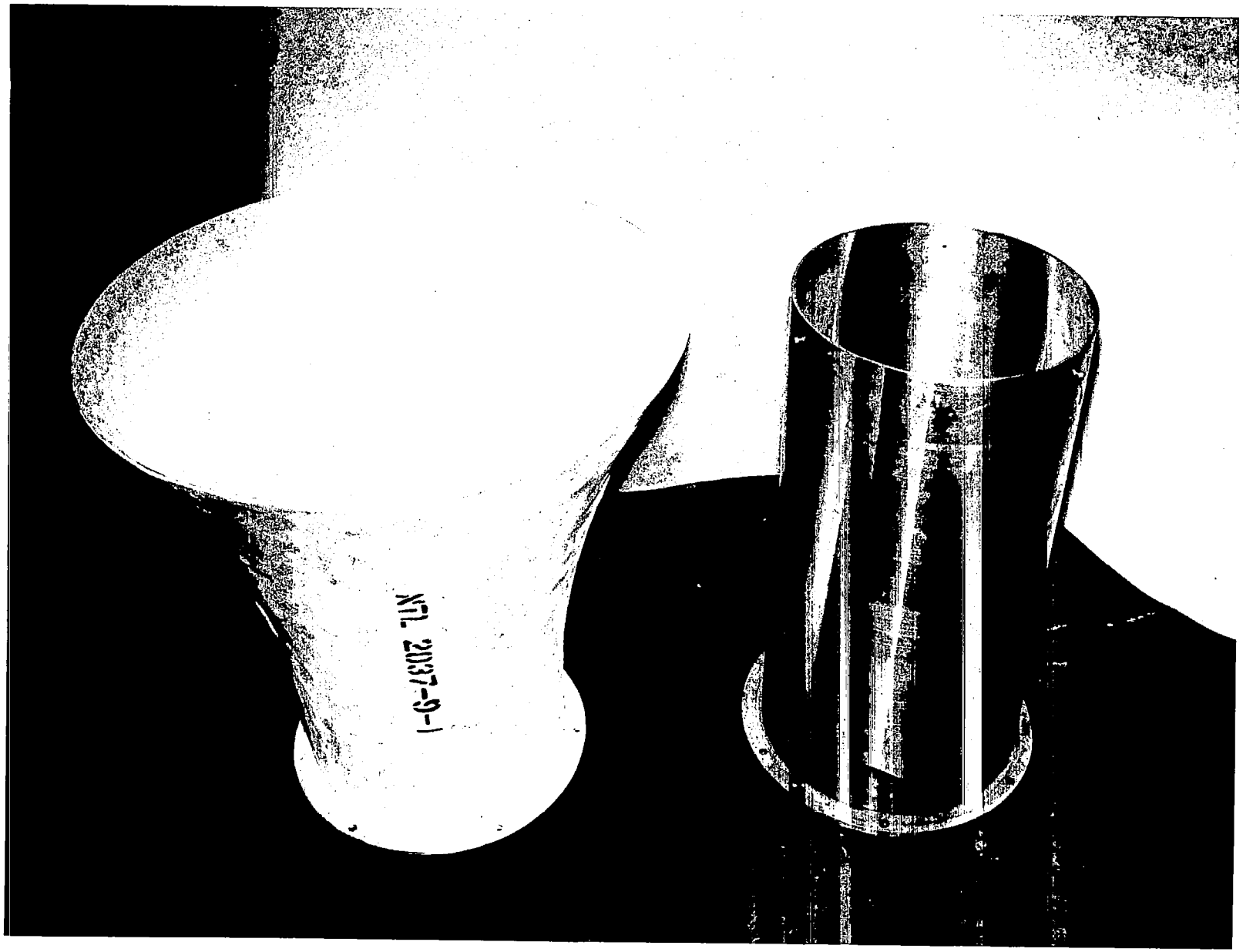

Figure 6. – Exponential and Straight Pipe Inlets

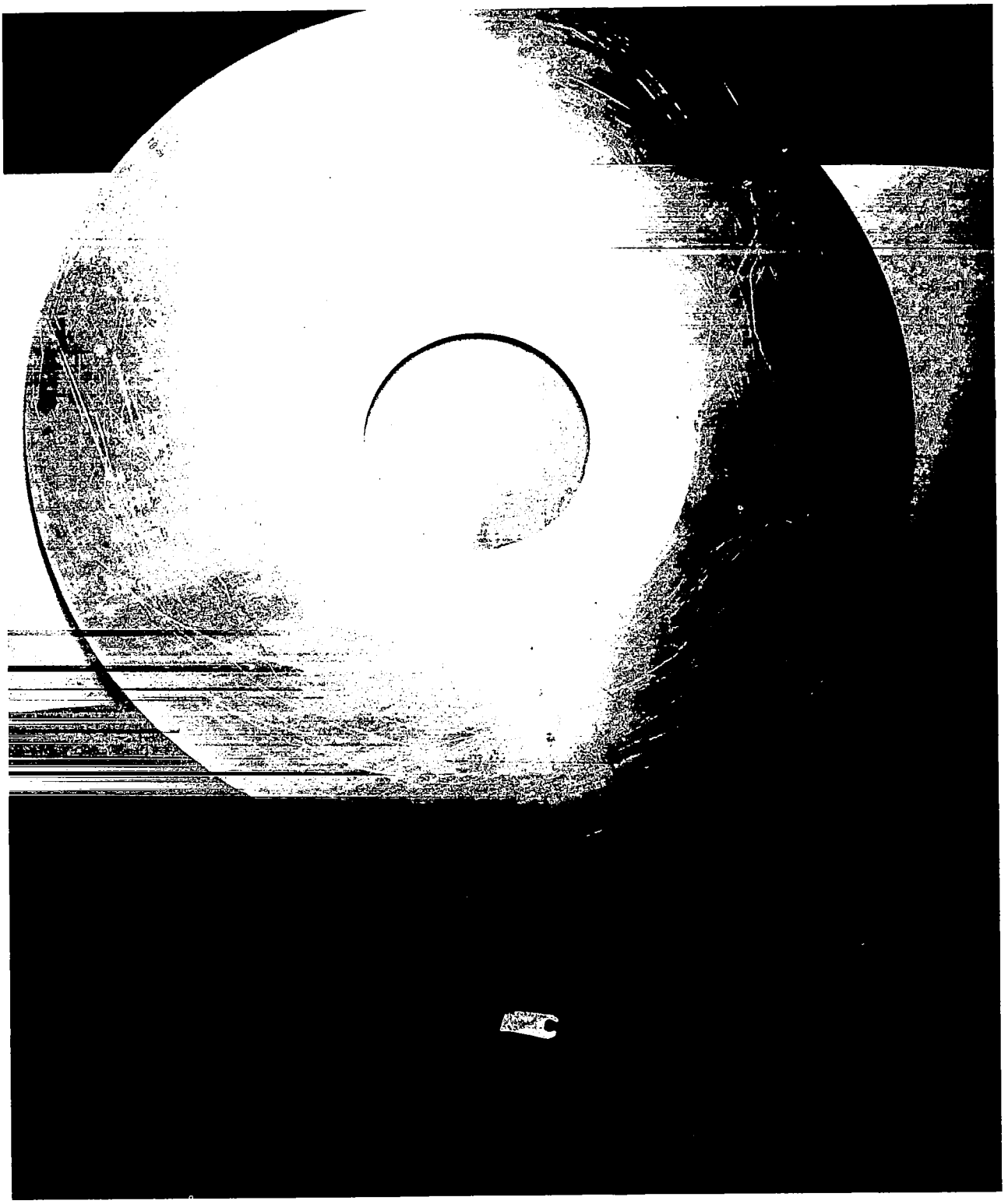

Figure 7. – Large and Small Baffles for the Straight Pipe Inlet

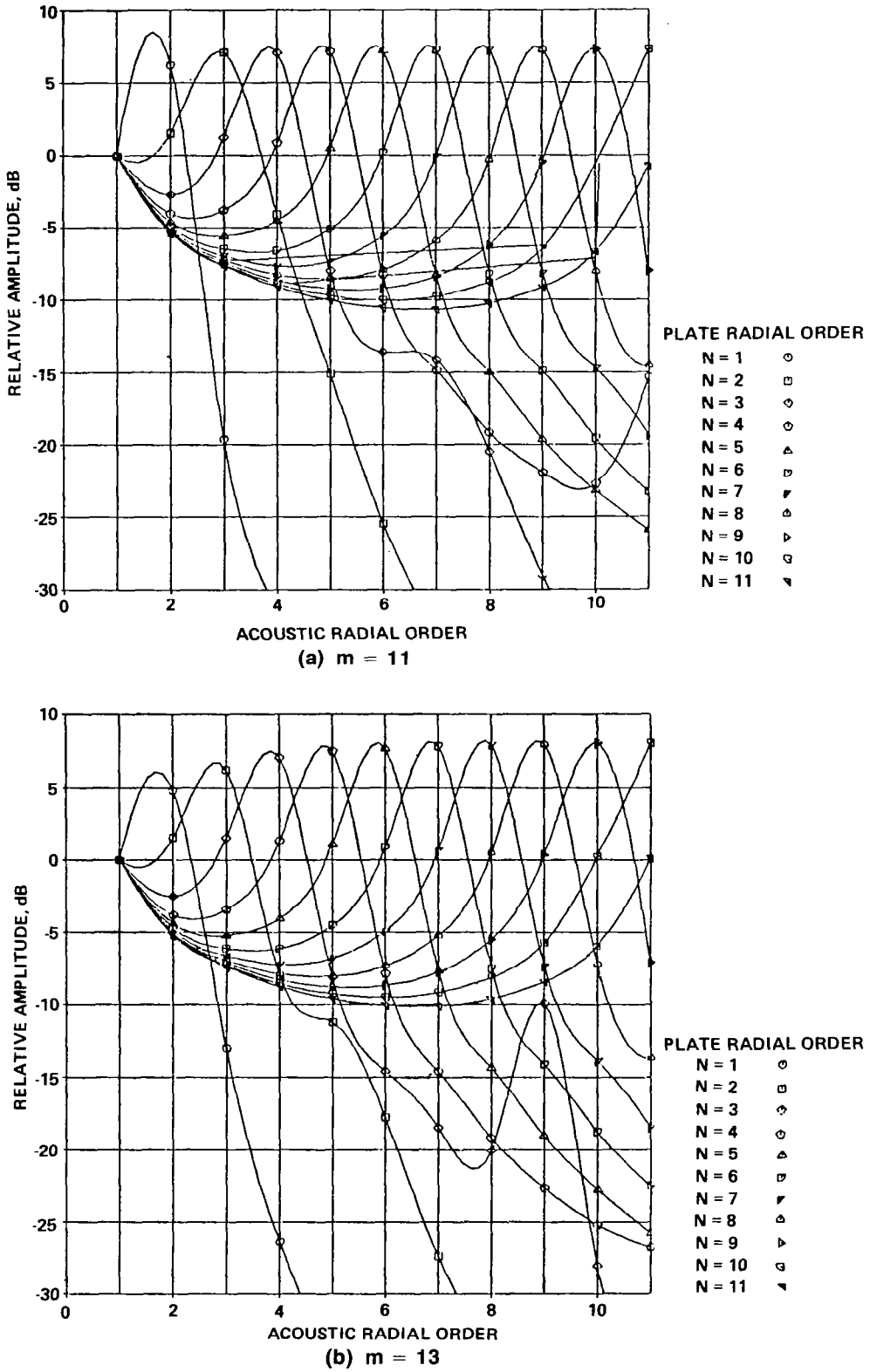

Figure 8. – Estimate of Excited Acoustic Mode Relative Amplitudes

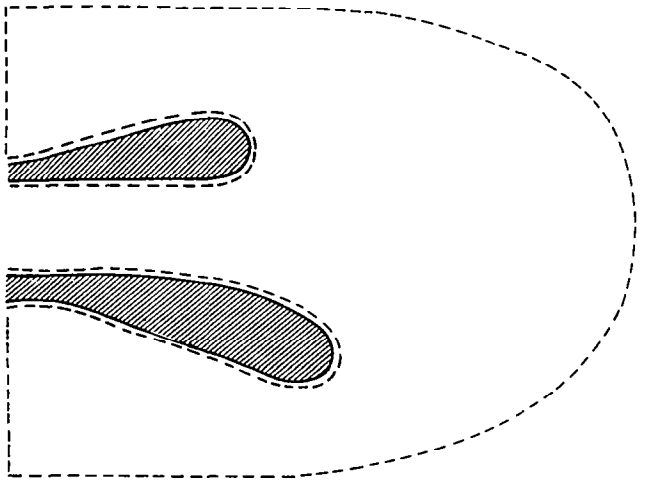

(a) LEVINE-SCHWINGER MODEL

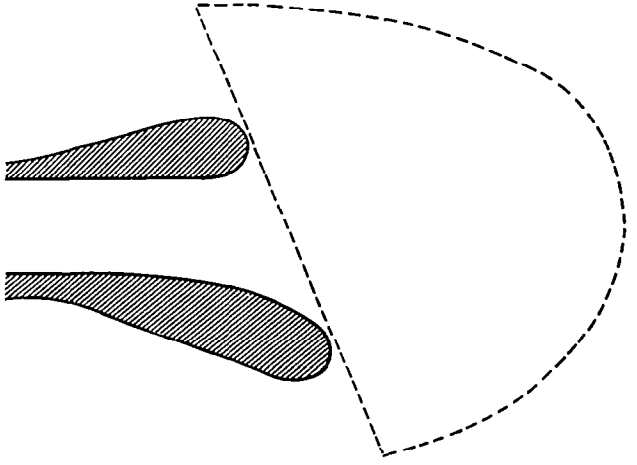

(c) INNER-OUTER REGION MODEL 2

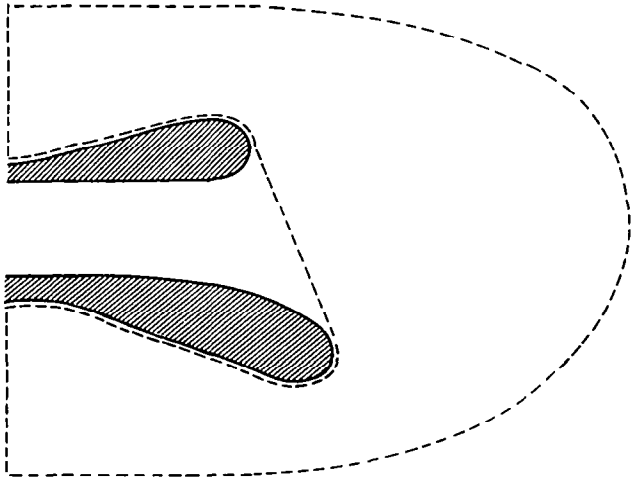

(b) INNER-OUTER REGION MODEL 1

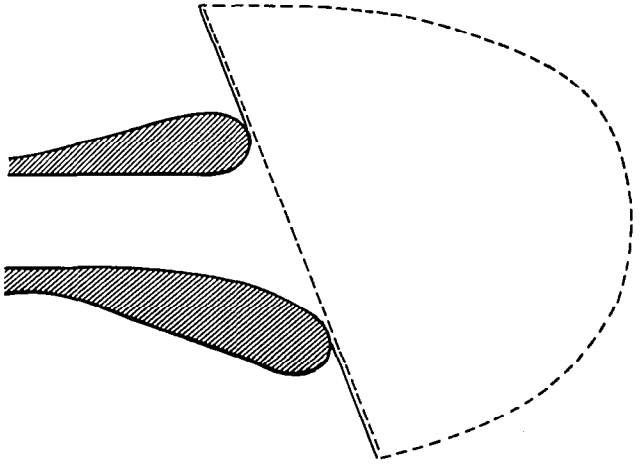

(d) INNER-OUTER REGION MODEL WITH BAFFLE

Figure 9. – Surface for Green's Theorem

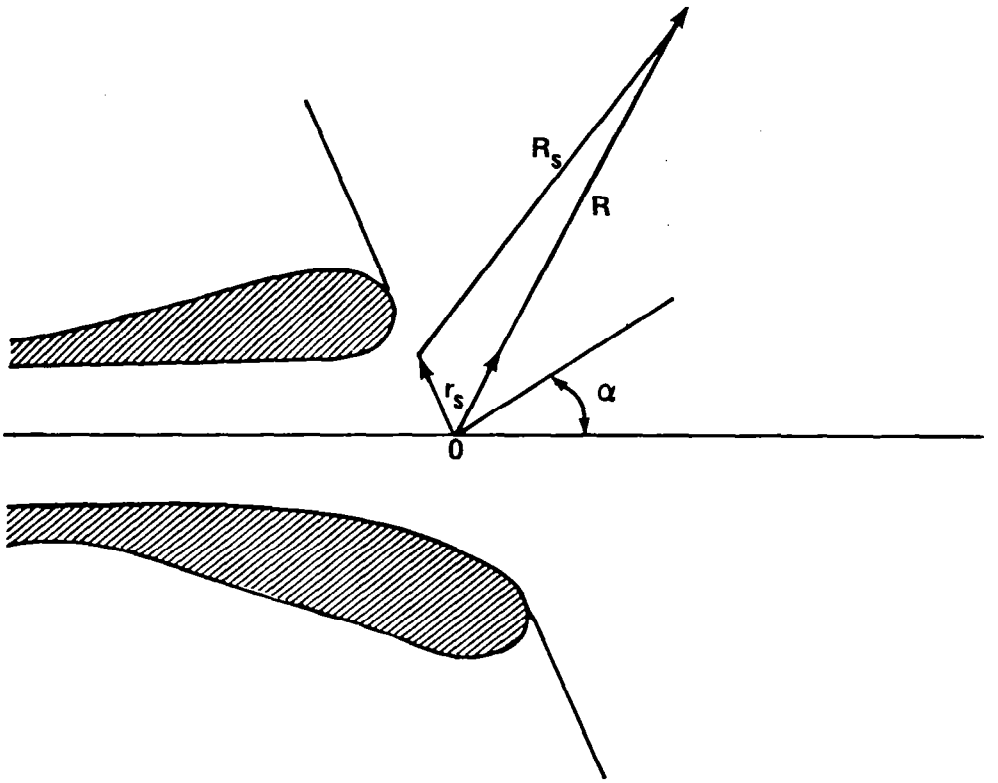

Figure 10. – Position Vectors for Radiation Calculation

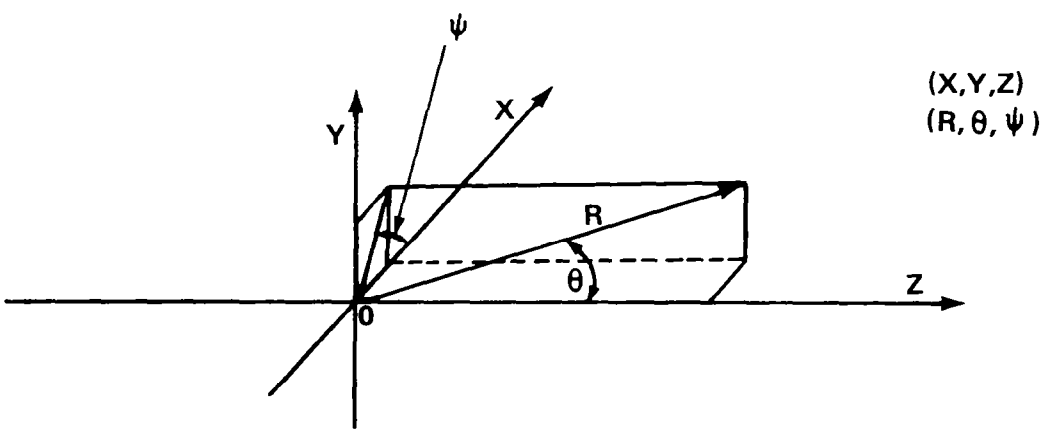

Figure 11. – Coordinate System

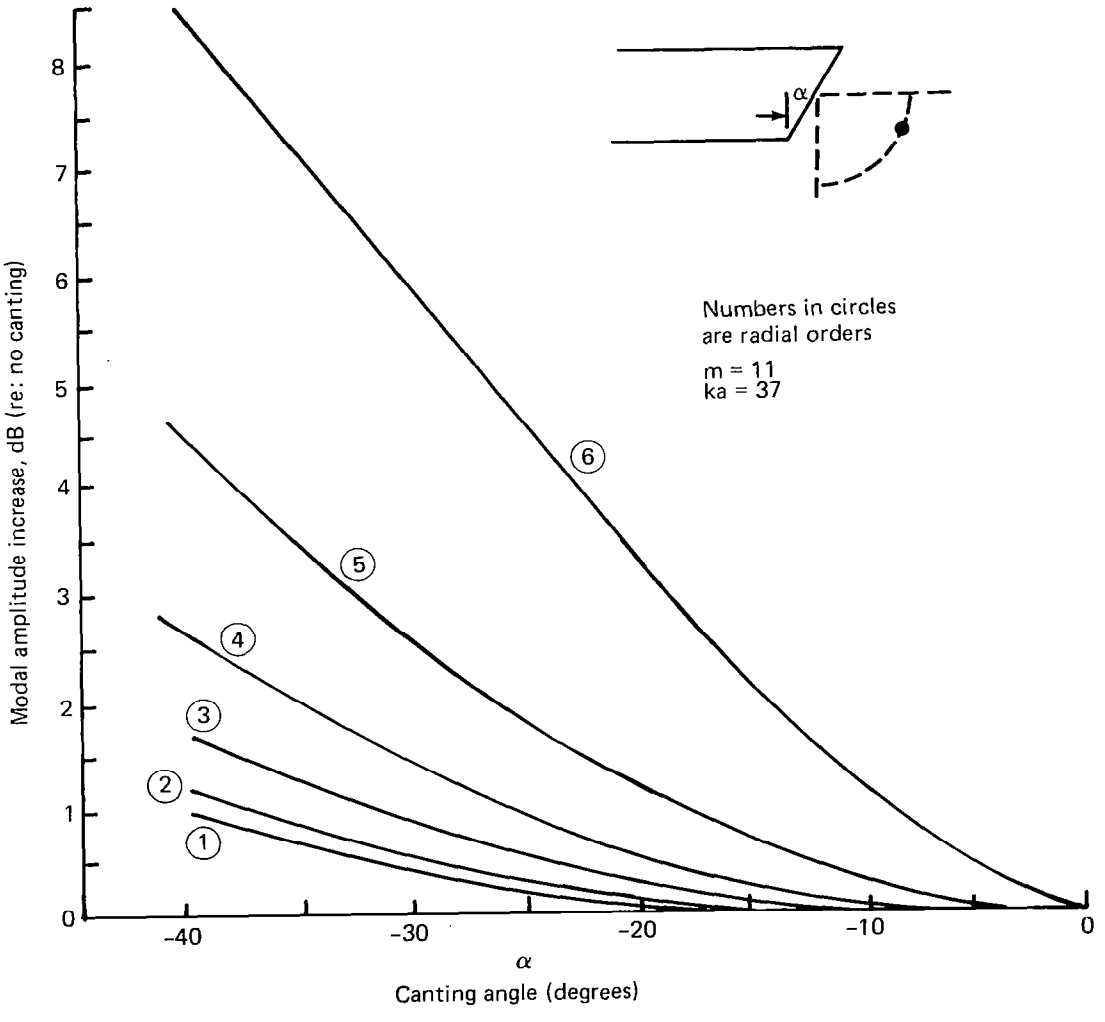

Figure 12. – Variation of Peak Values With Canting Angle (–VE as Sketched)

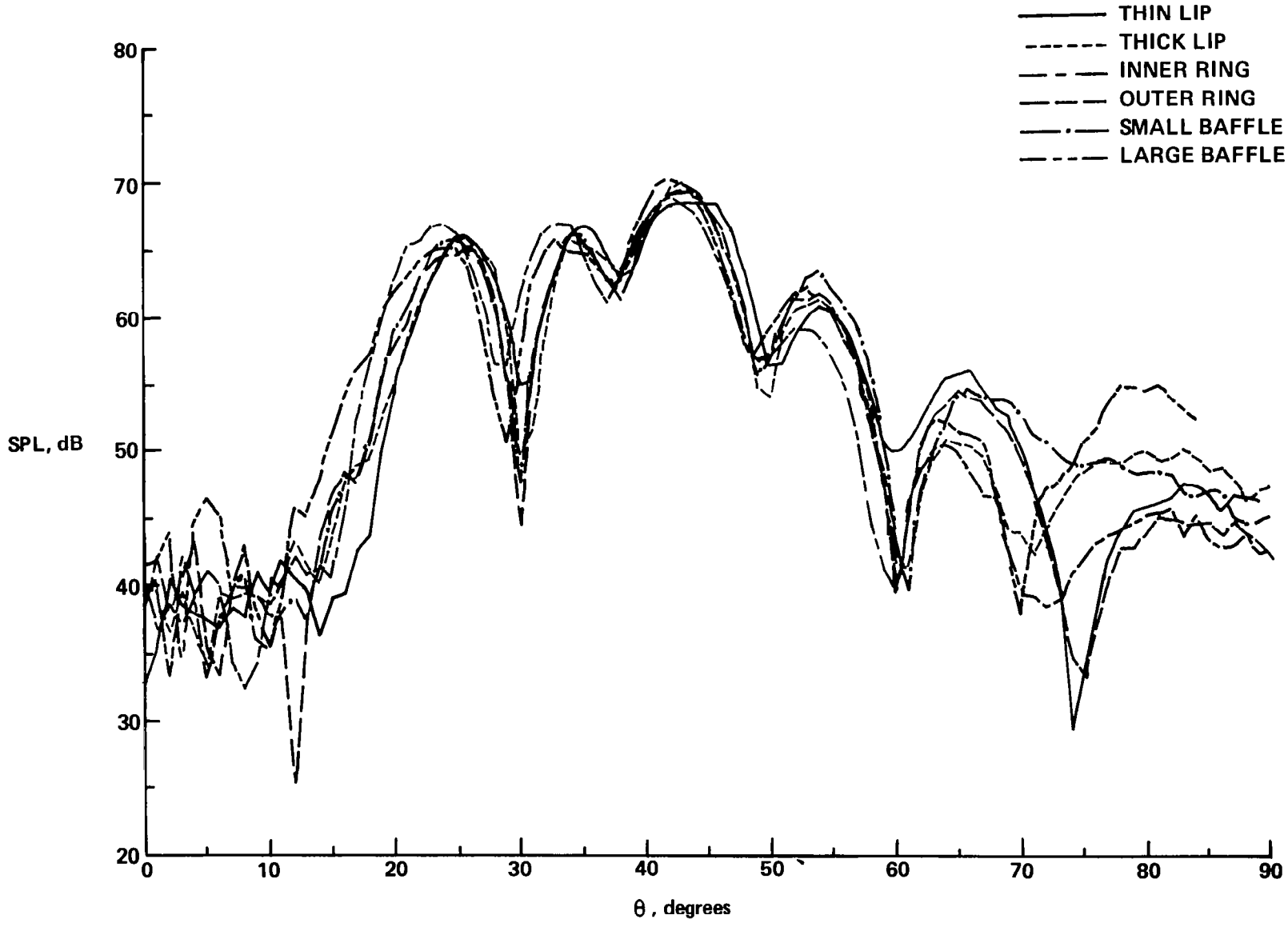

Figure 13. – Experimental Directivity Patterns of the Straight Pipe Inlets for the Plate Mode (11,3)

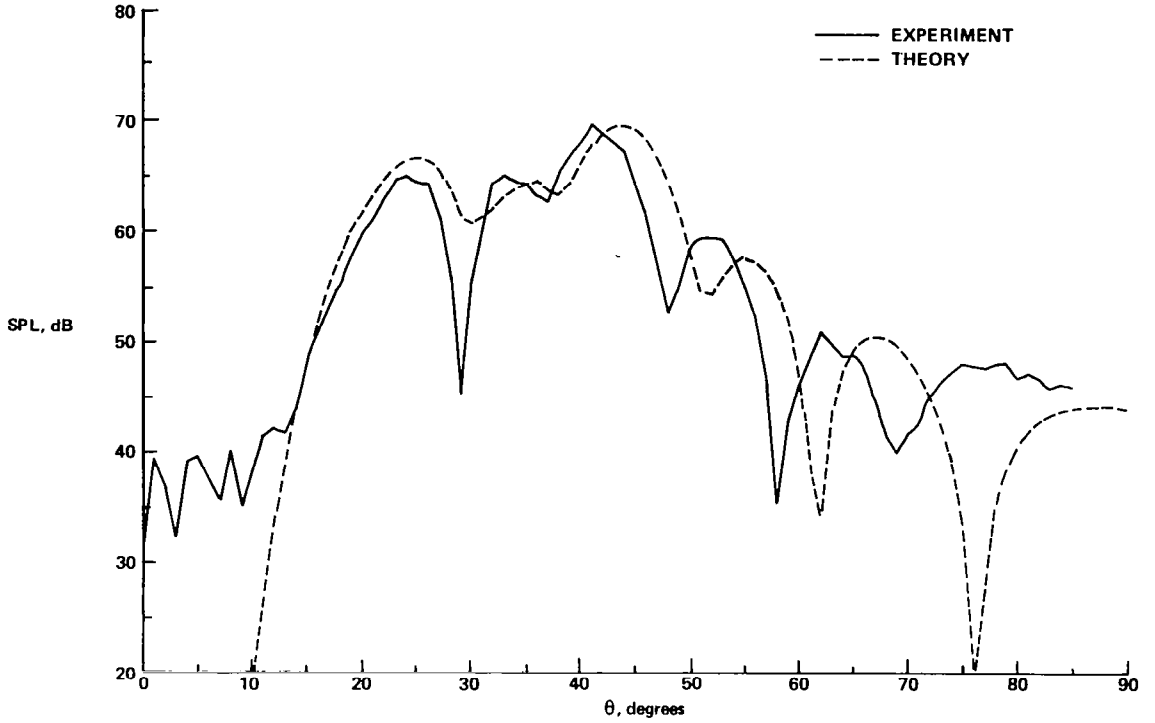

(a) THICK LIP

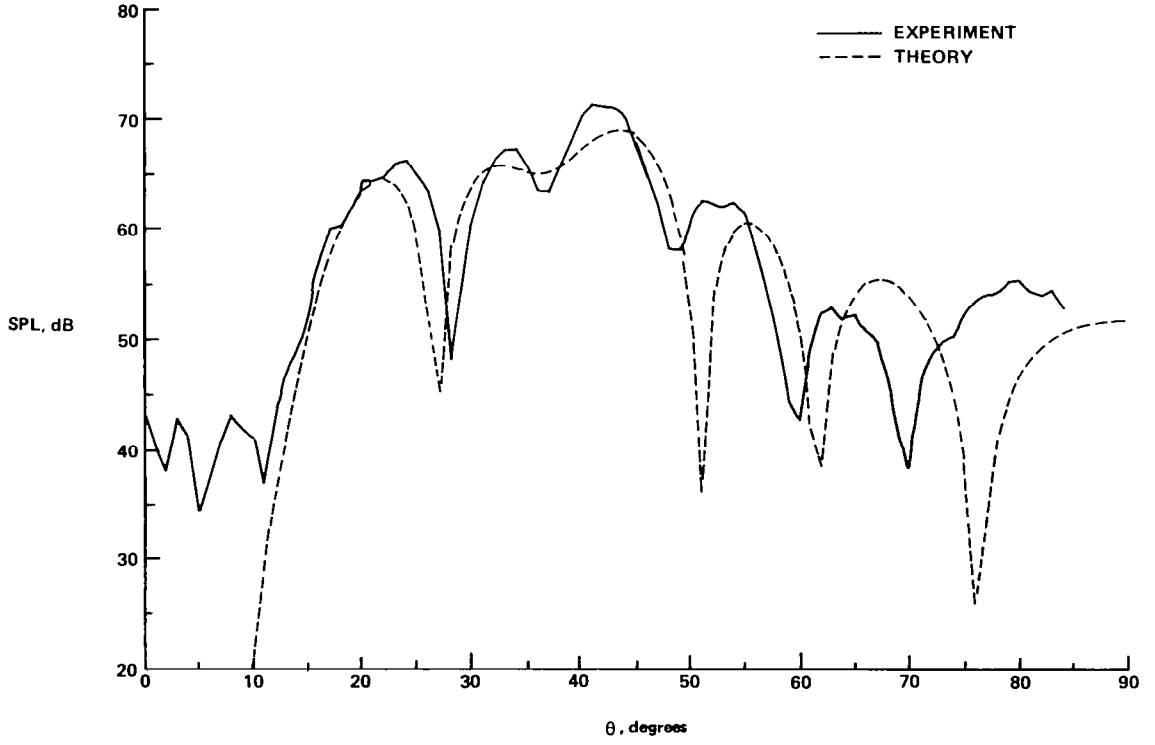

(b) LARGE BAFFLE

Figure 14. – Standard Theory Versus Experiment, Straight Pipe Inlet for Plate Mode (11,3)

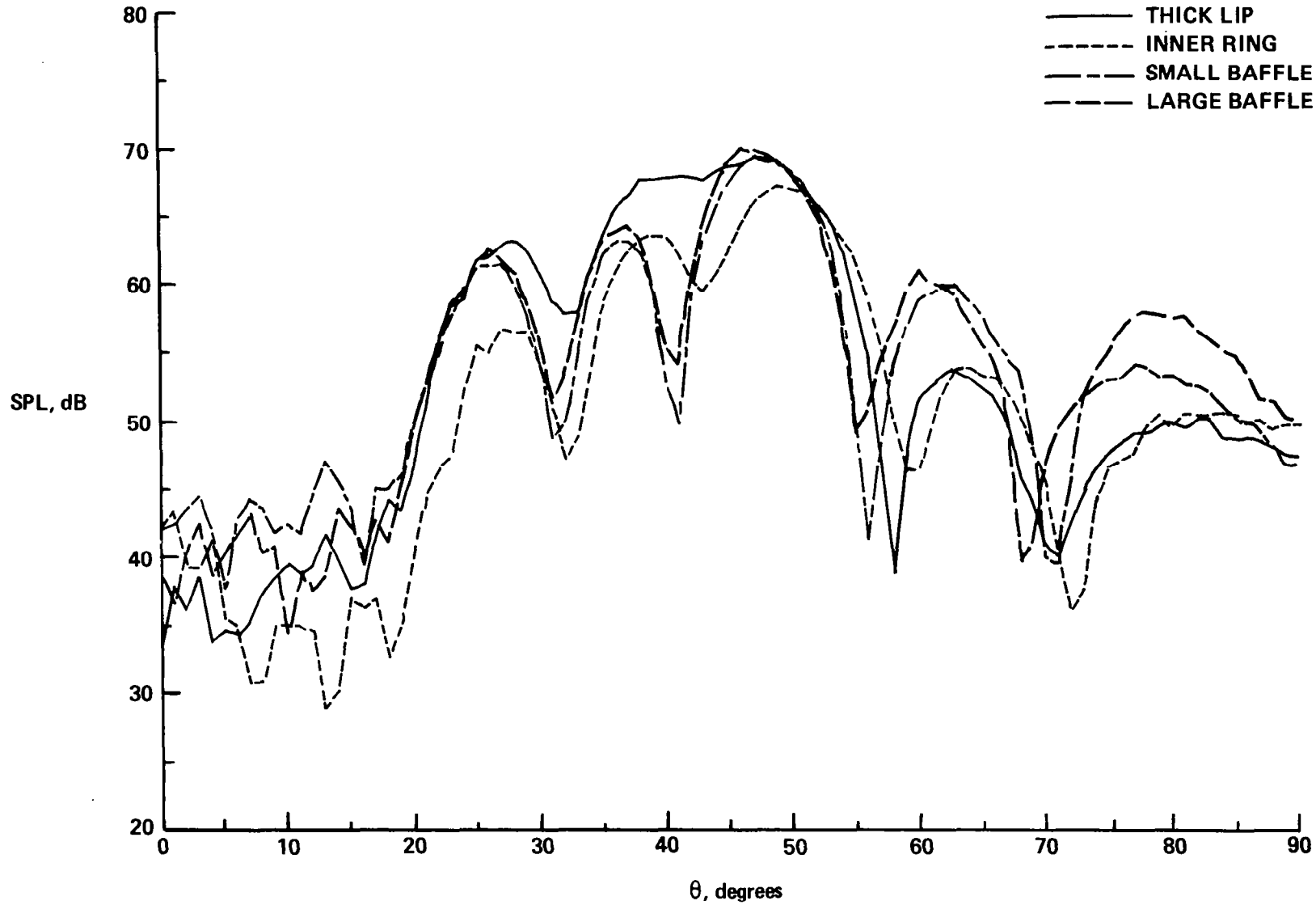

Figure 15. – Experimental Directivity Patterns of the Straight Pipe Inlets for the Plate Mode (13,2)

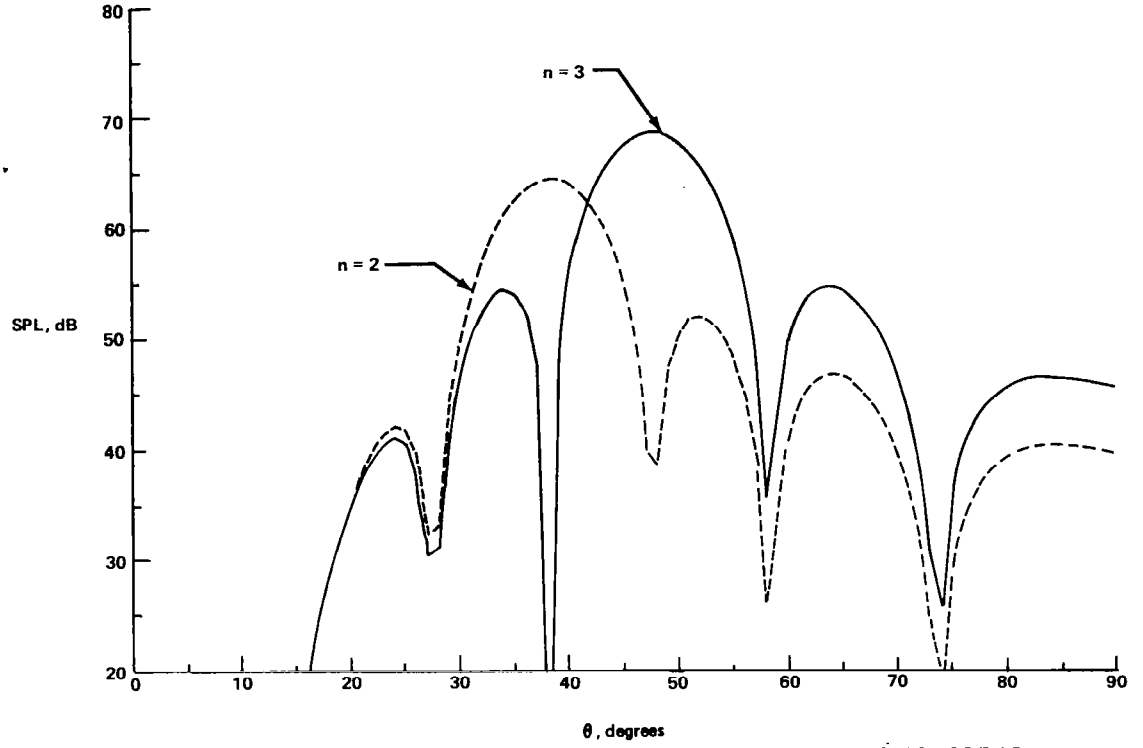

(a) THEORETICAL PATTERNS FOR THE n= 2 AND n = 3 ACOUSTIC MODES

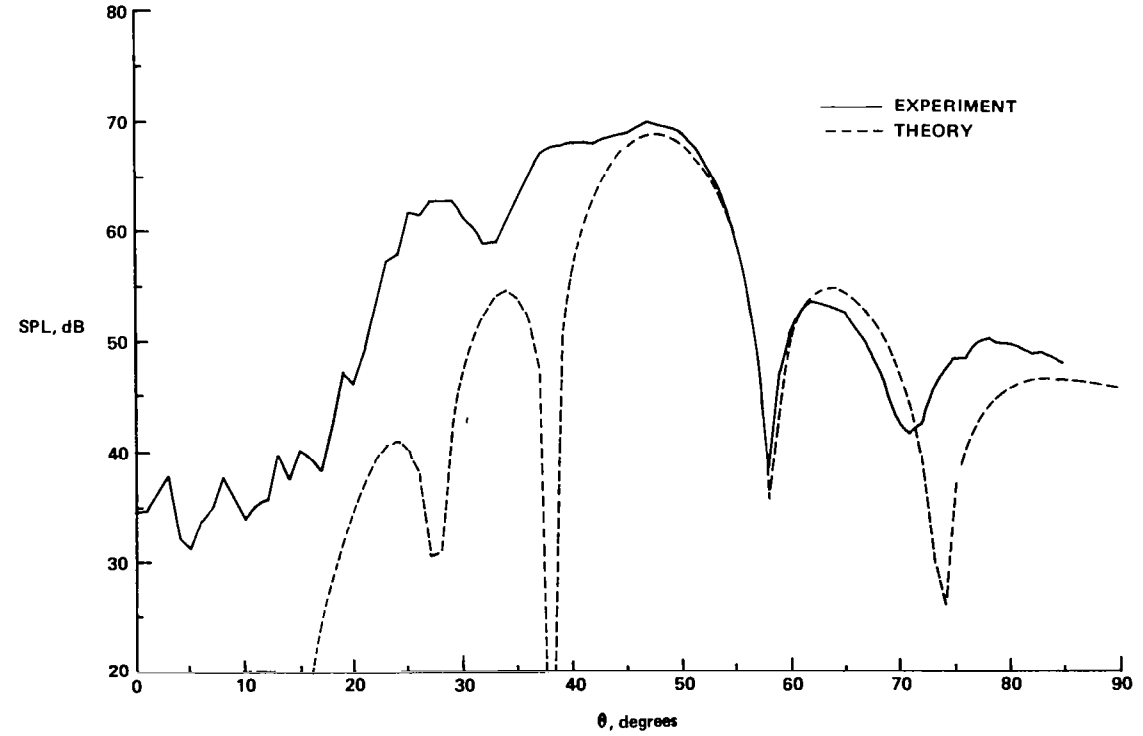

(b) STANDARD THEORY (WITH SINGLE ACOUSTIC MODE n = 3) VERSUS EXPERIMENT (THICK LIP)

Figure 16. – Directivity of Straight Pipe Inlet for the Plate Mode (13, 2)

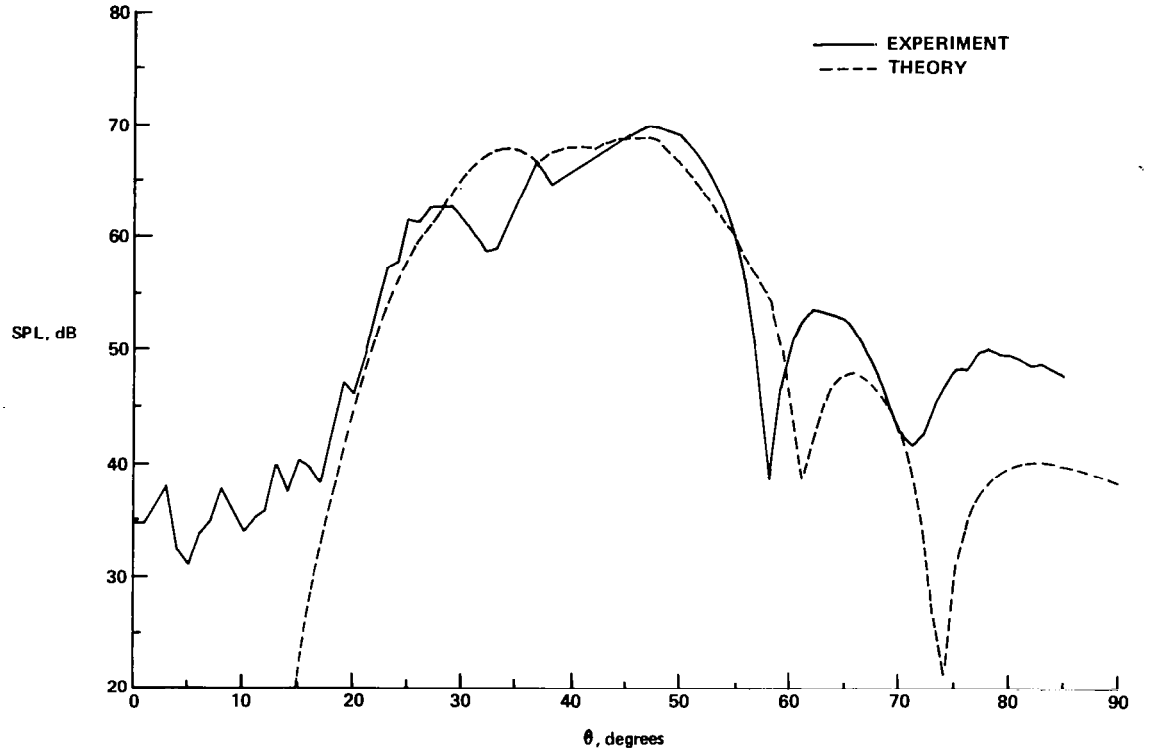

(a) THICK LIP

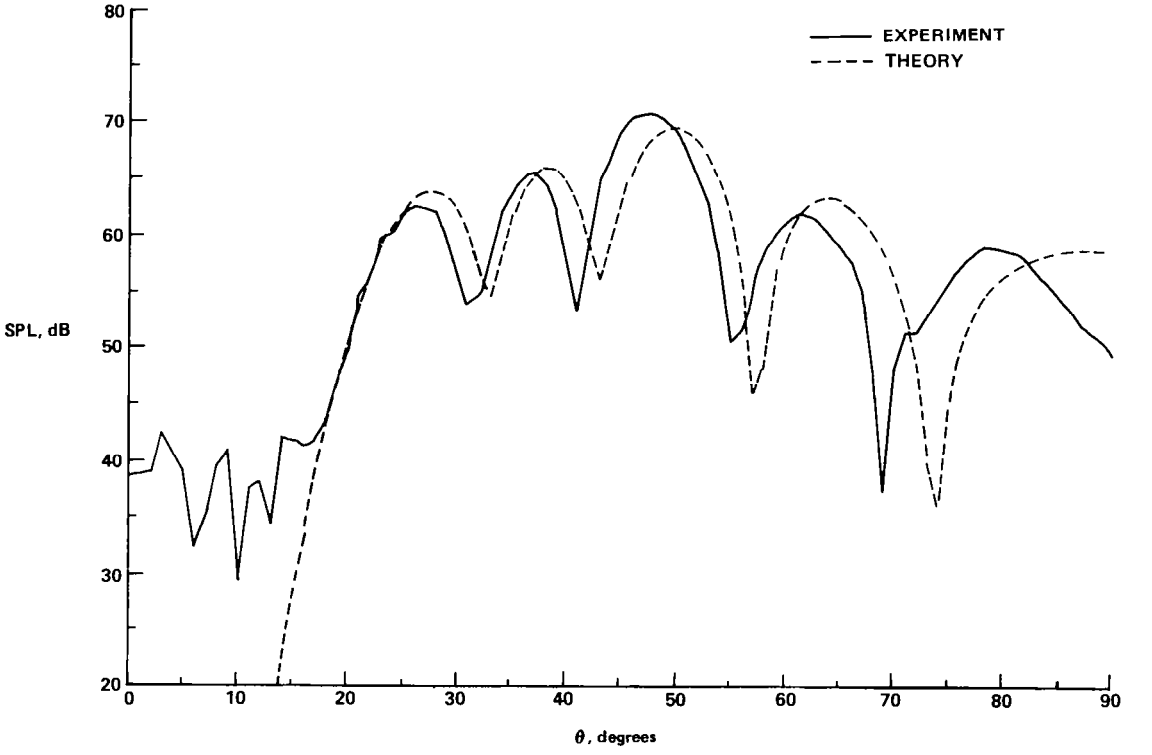

(b) LARGE BAFFLE

Figure 17. – Standard Theory Versus Experiment, Straight Pipe Inlet for Plate Mode (13.2)

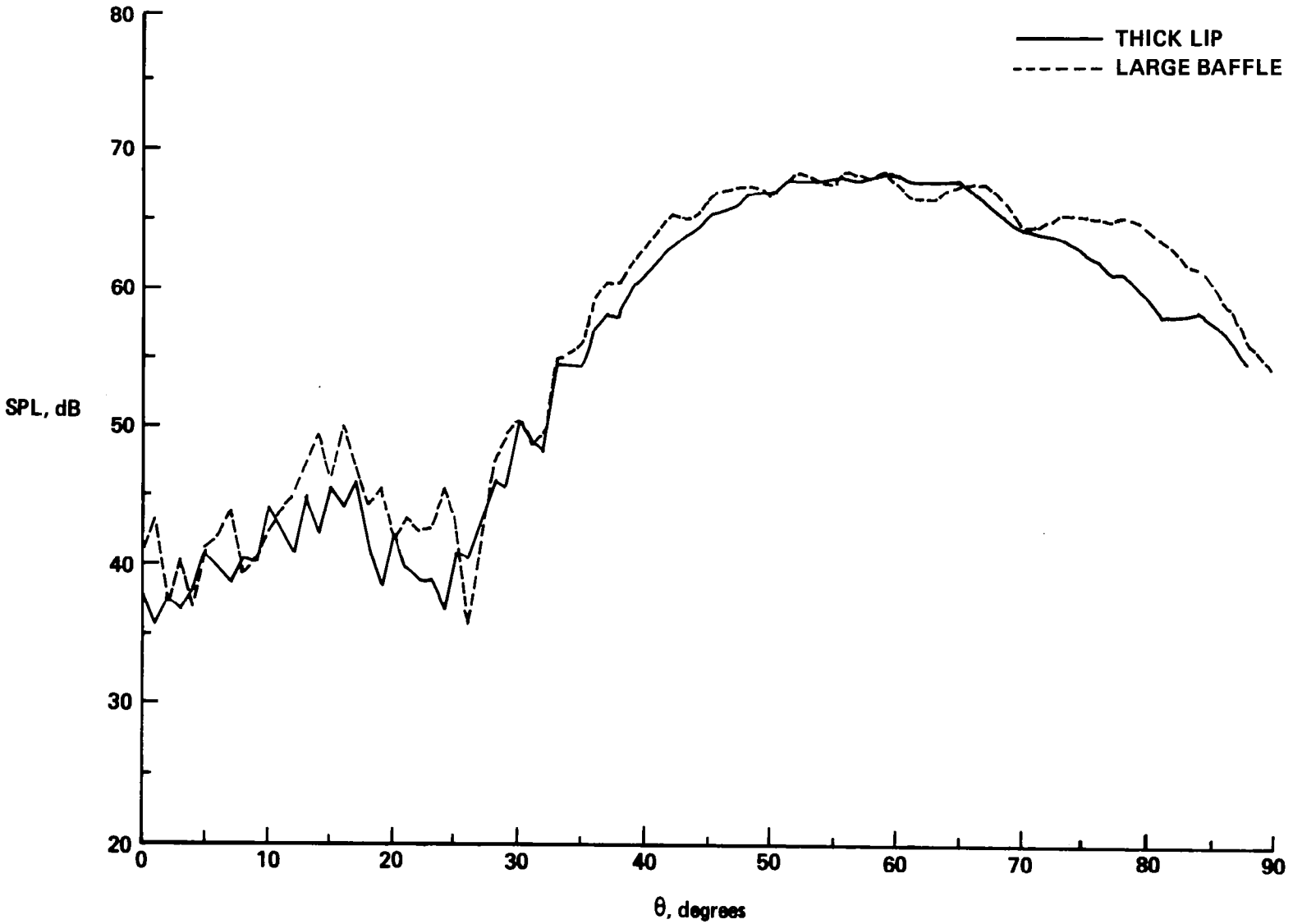

Figure 18. – Experimental Directivity Patterns of the Straight Pipe Inlets for the Plate Mode (13,1)

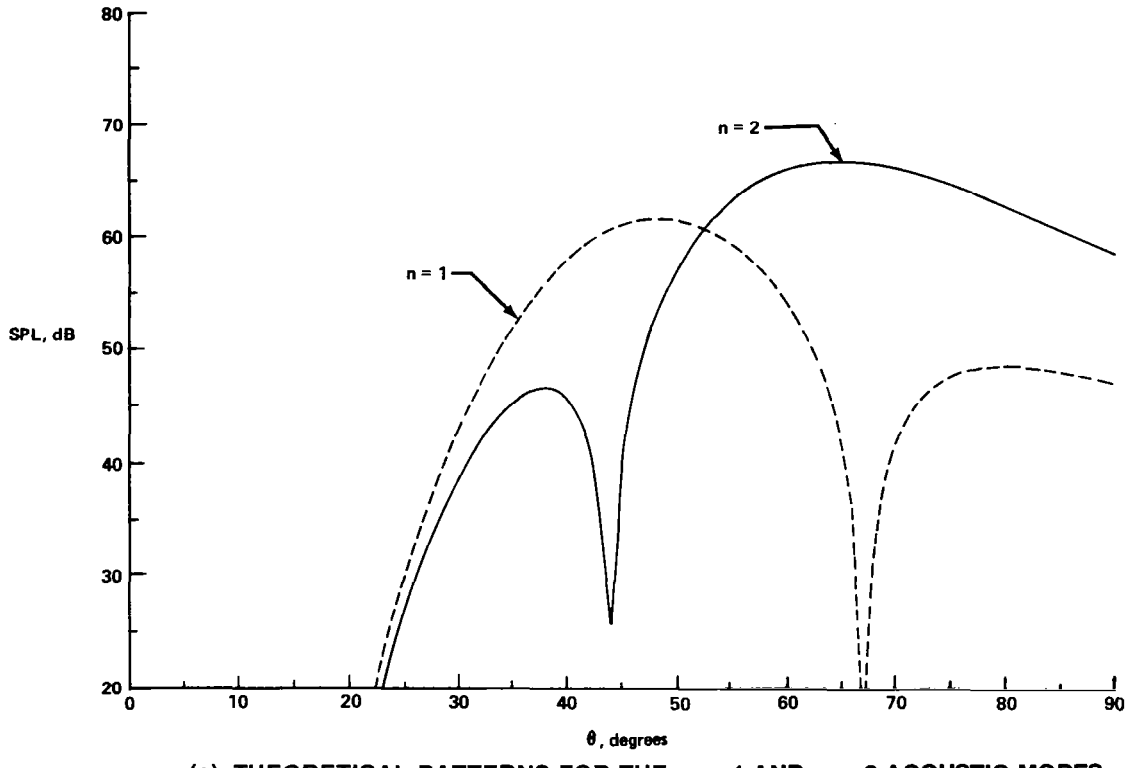

(a) THEORETICAL PATTERNS FOR THE n = 1 AND n = 2 ACOUSTIC MODES

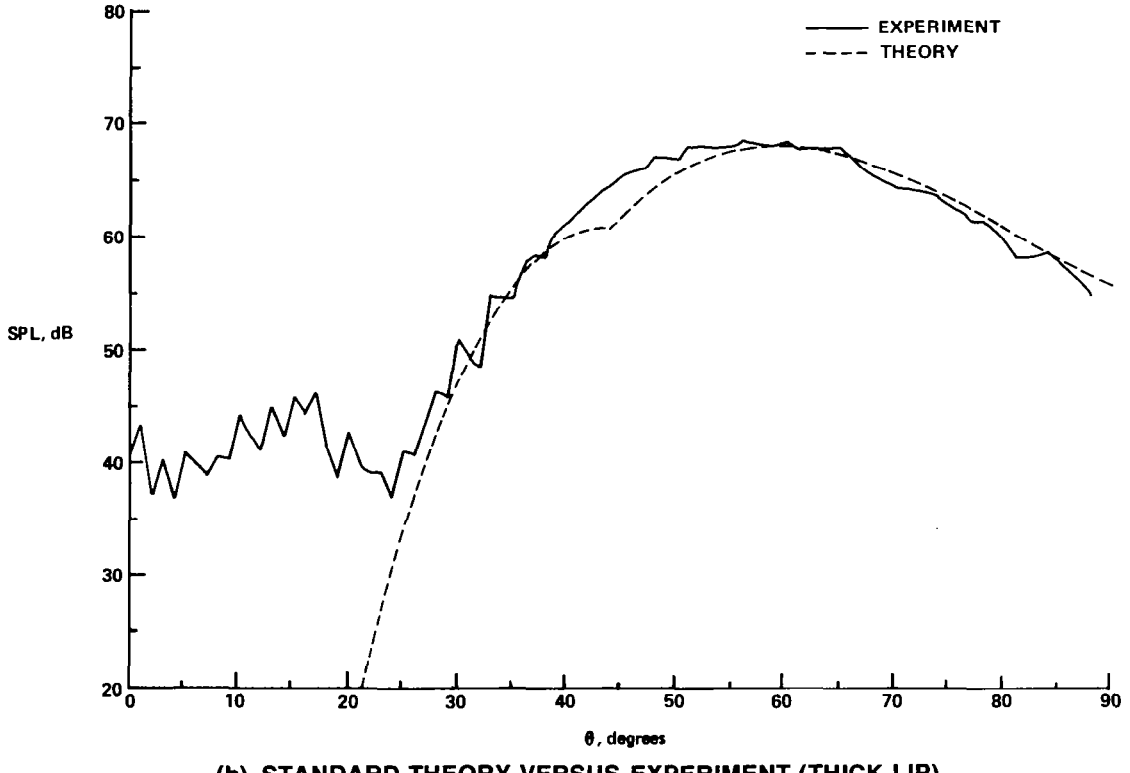

(b) STANDARD THEORY VERSUS EXPERIMENT (THICK LIP)

Figure 19. – Directivity of Straight Pipe Inlet for the Plate Mode (13,1)

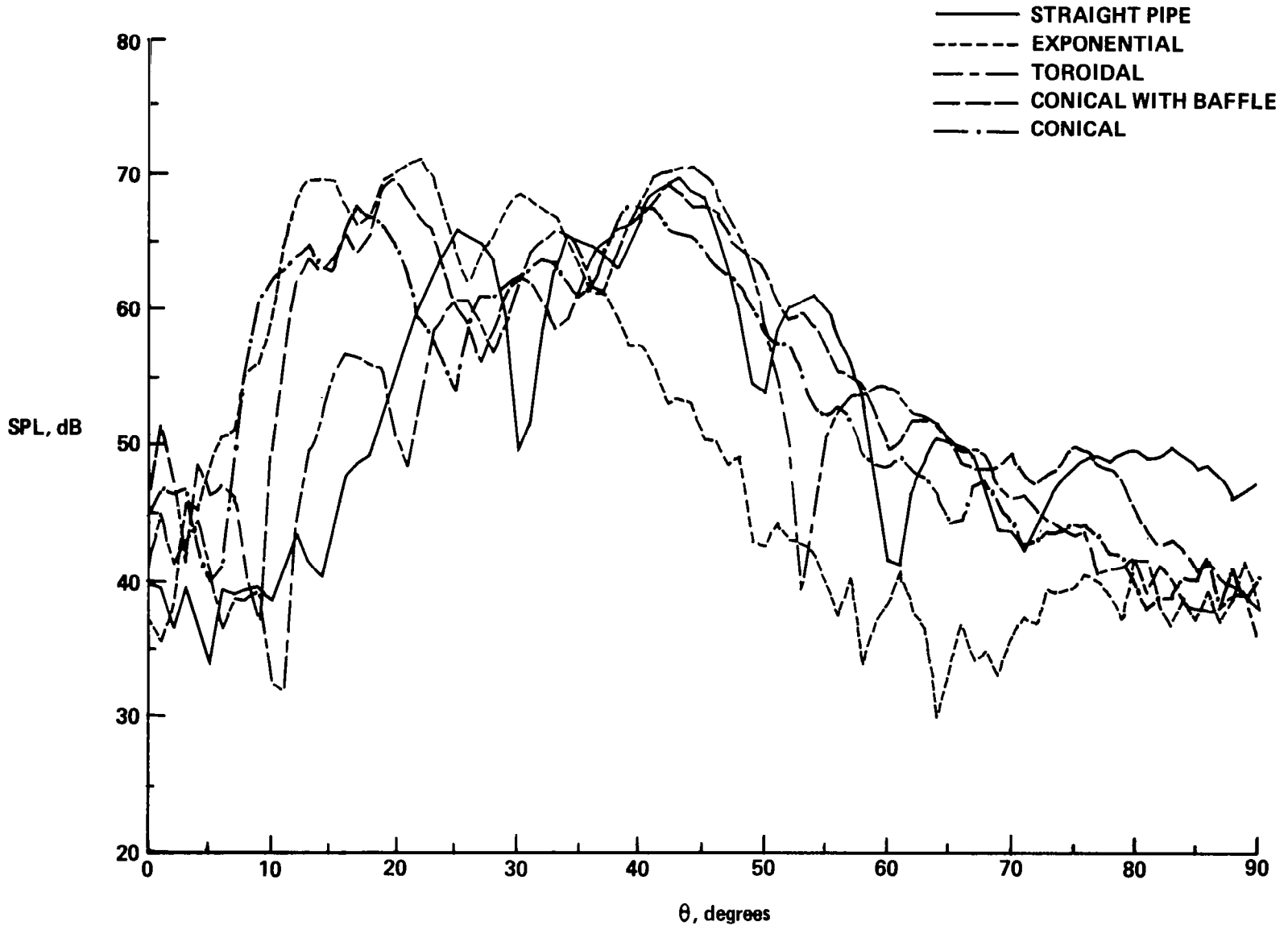

Figure 20. – Experimental Directivity Patterns of the Symmetric Inlets for the Plate Mode (11,3)

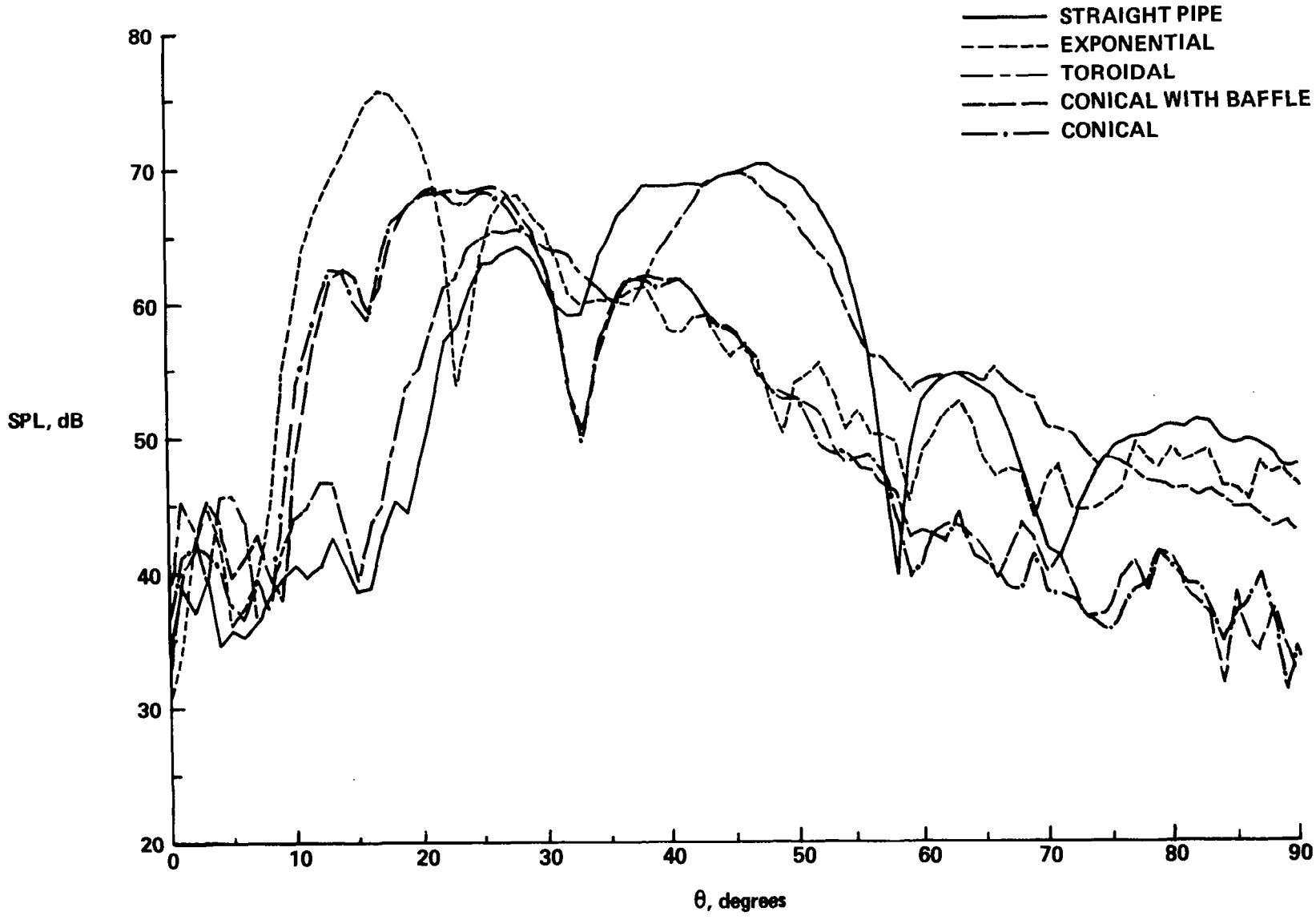

Figure 21. – Experimental Directivity Patterns of the Symmetric Inlets for the Plate Mode (13,2)

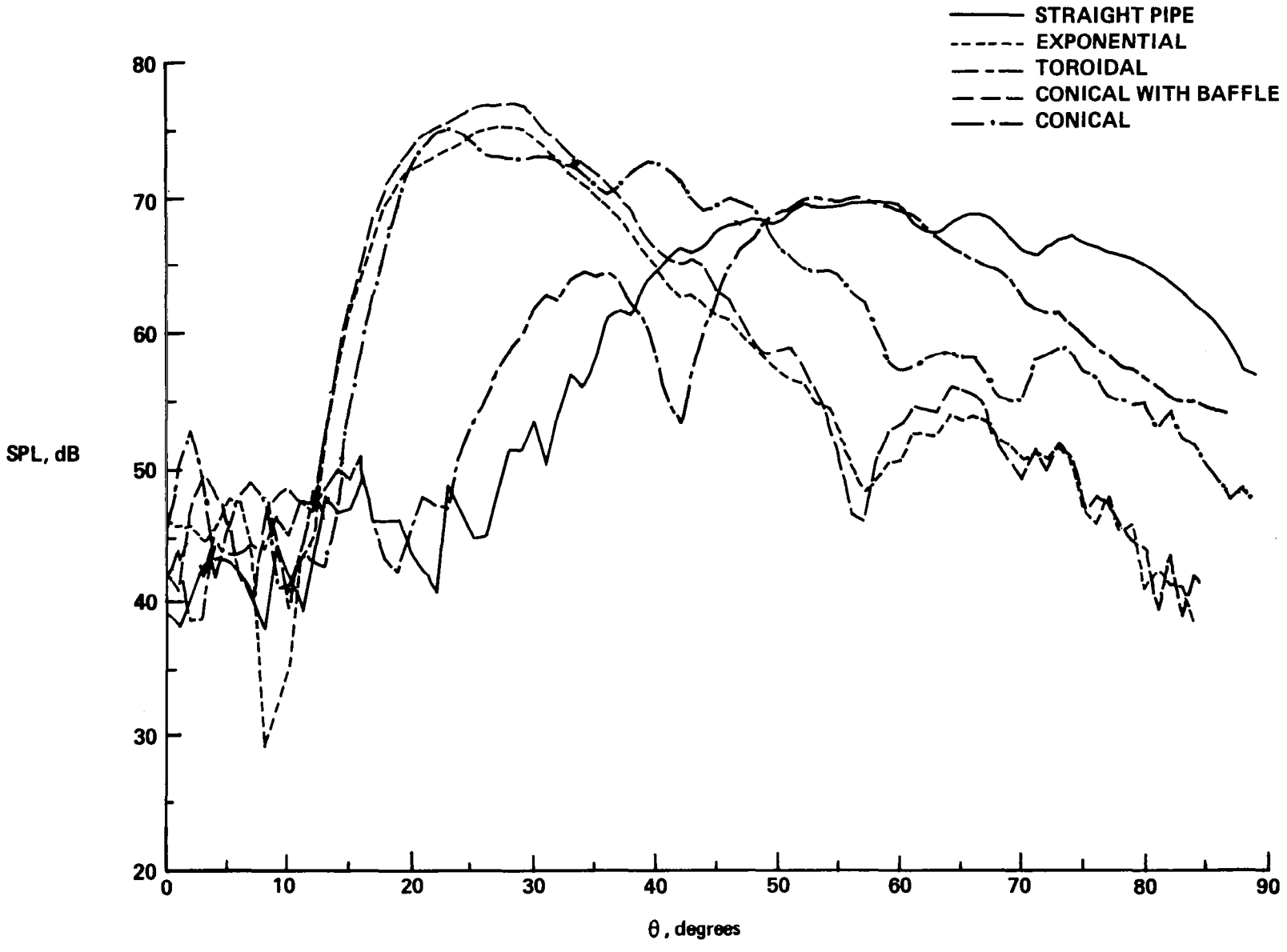

Figure 22. – Experimental Directivity Patterns of the Symmetric Inlets for the Plate Mode (13,1)

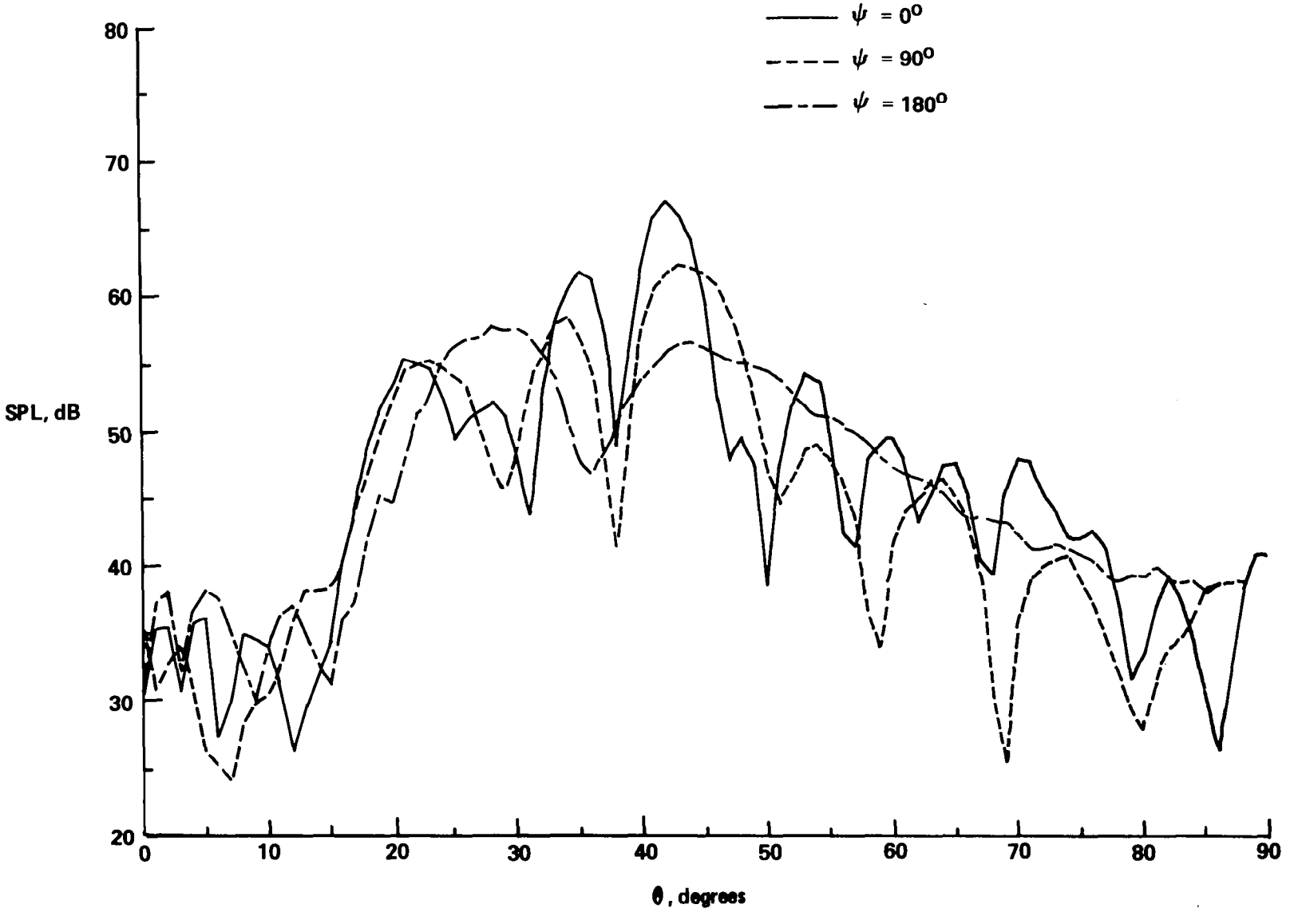

Figure 23. – Experimental Directivity Patterns of the Asymmetric Inlet for Plate Mode (11,3)

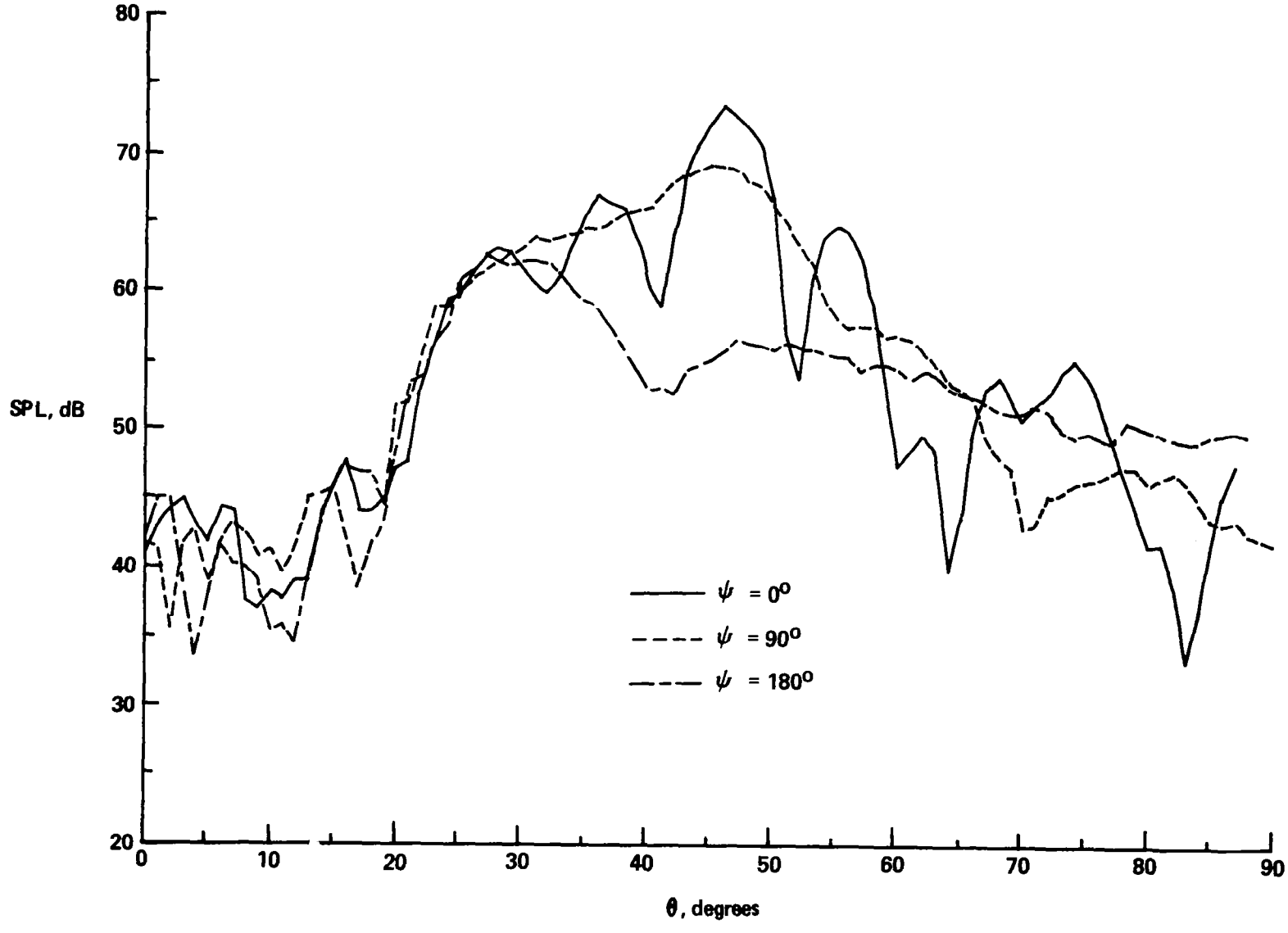

Figure 24. – Experimental Directivity Patterns of the Asymmetric Inlet for Plate Mode (13,2)

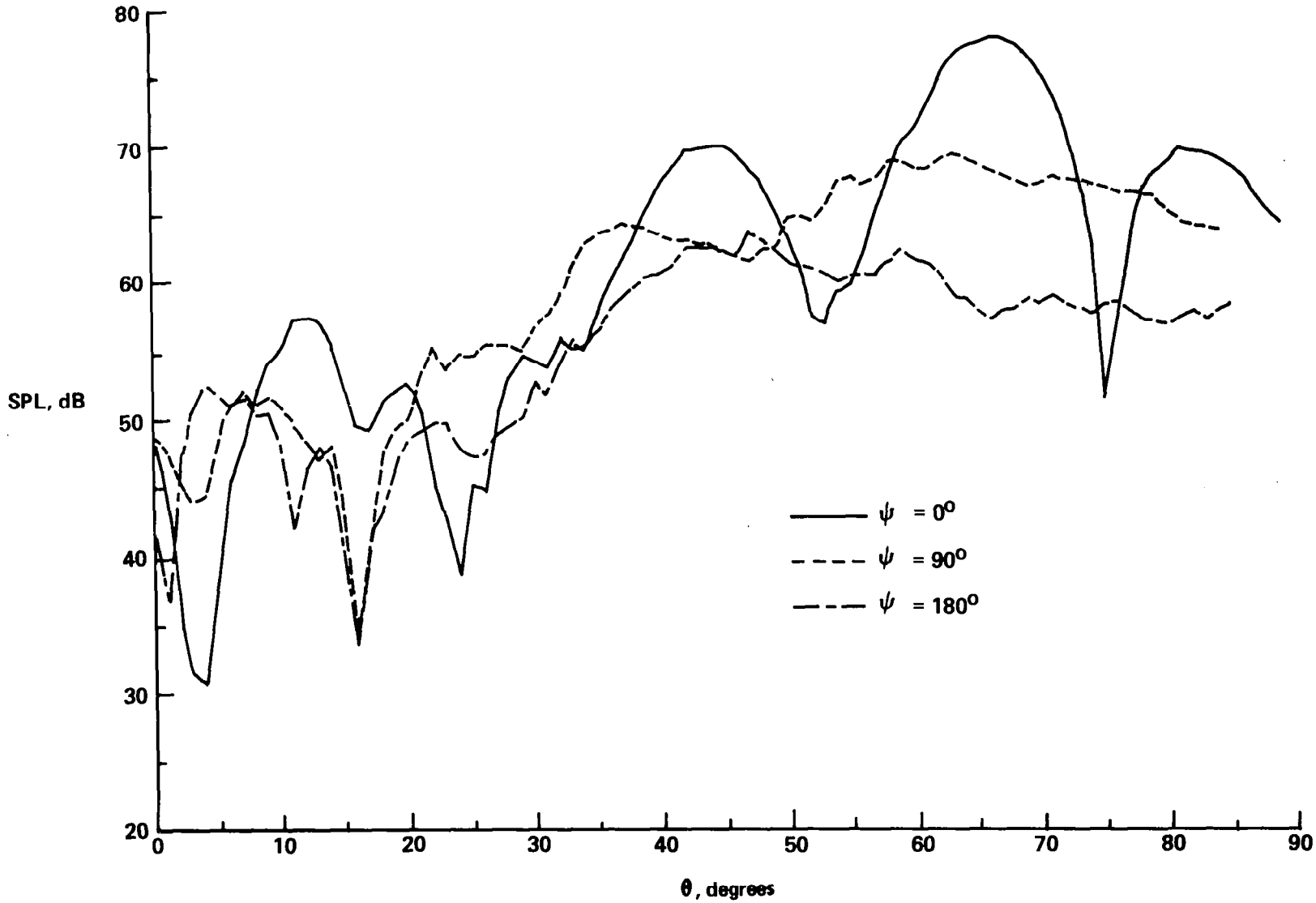

Figure 25. – Experimental Directivity Patterns of the Asymmetric Inlet for Plate Mode (13,1)

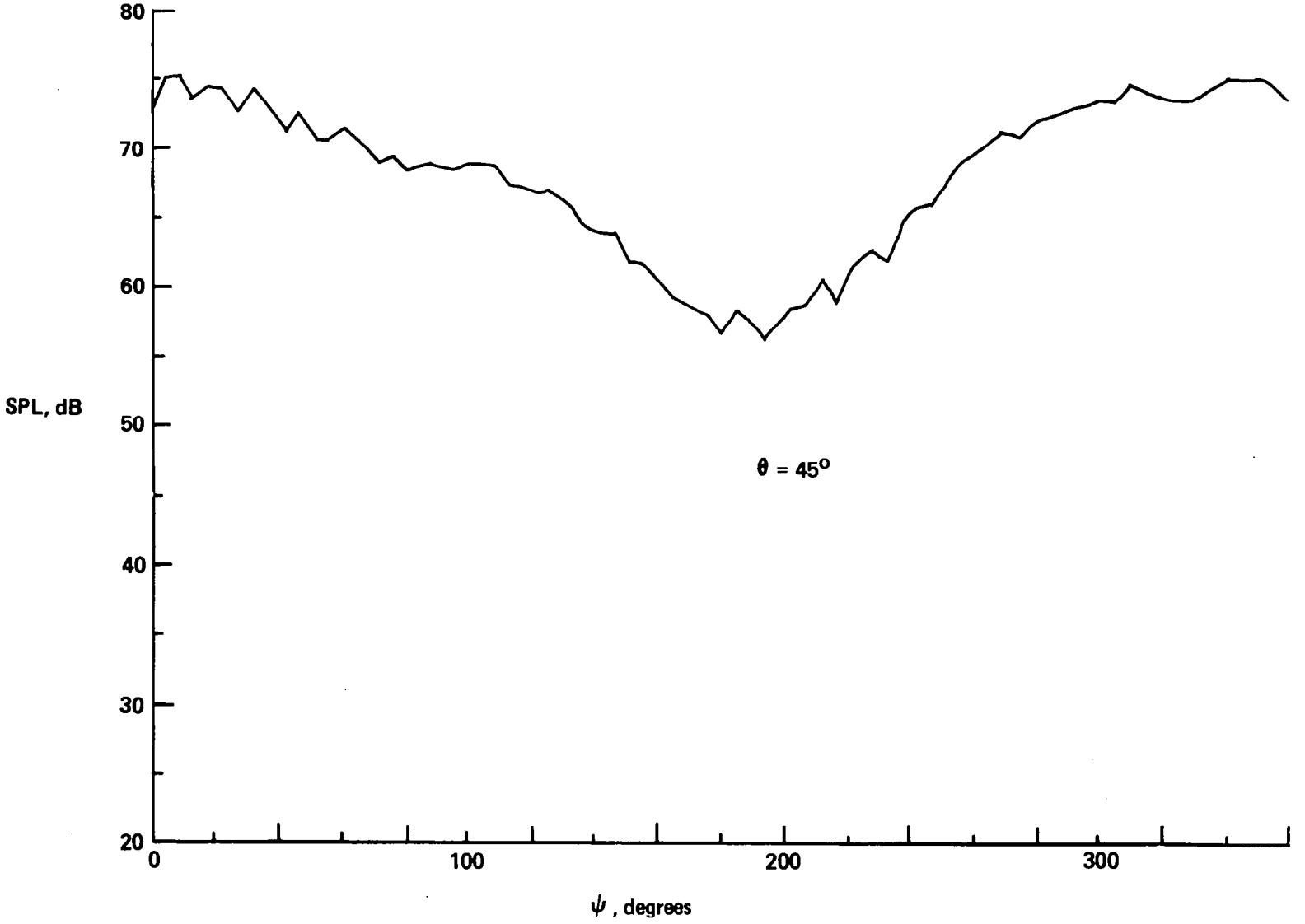

Figure 26. – Experimental Peak SPL Versus Rotation Angle for Asymmetric Inlet, Plate Mode (13,2)

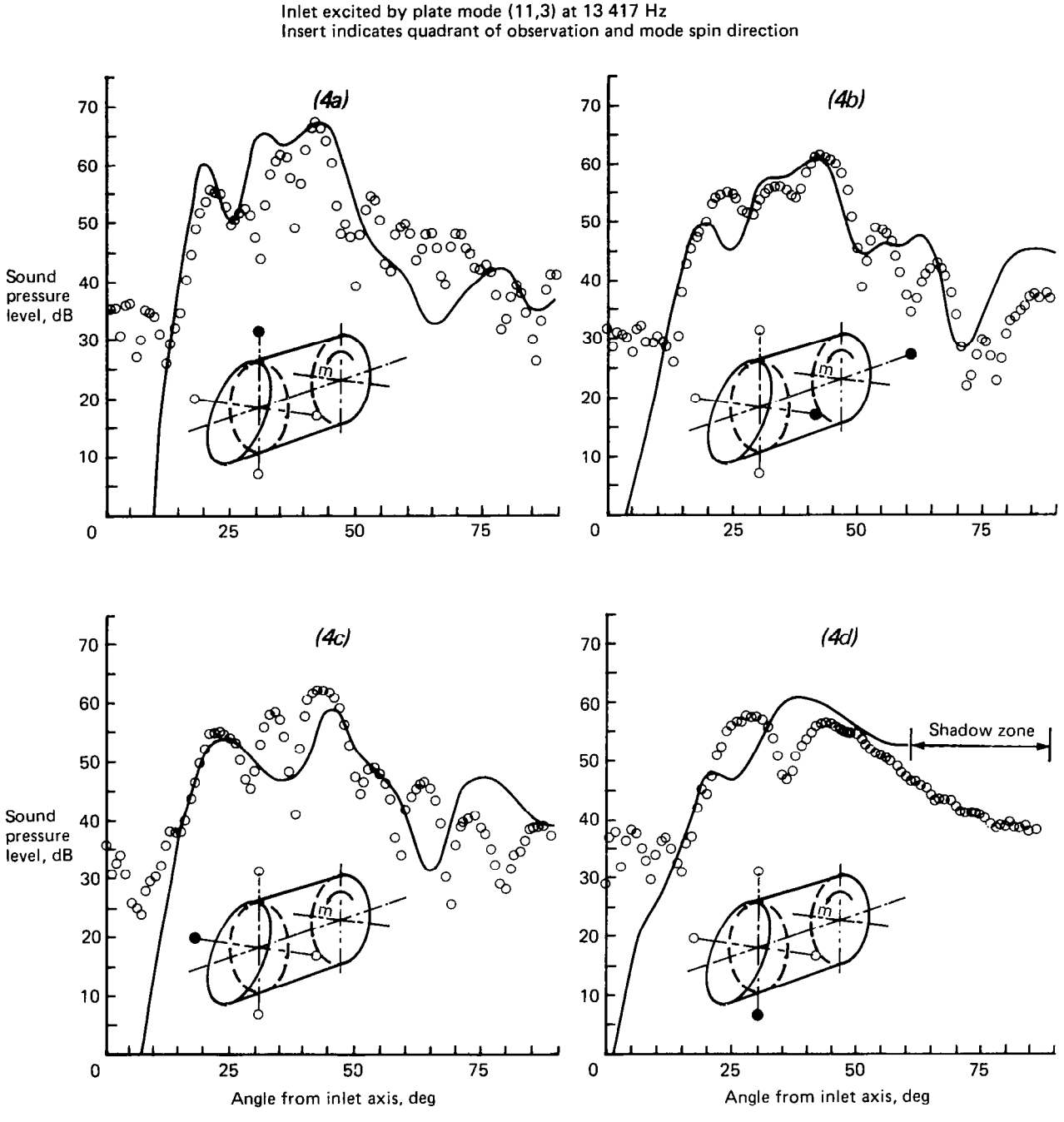

Figure 27. – Comparison Between Measured and Theoretical Radiation Patterns of Asymmetric Inlet

Table I

INLET SHAPES
Straight pipe, thin lip
Straight pipe, thick lip
Straight pipe, inner ring
Straight pipe, outer ring
Straight pipe, small baffle
Straight pipe, large baffle
Conical
Conical with baffle
Exponential
Toroidal
Straight pipe, asymmetric

SOURCE CONDITIONS	
Plate mode	Frequency
13,1	7.996 KHz
13,2	11.971 KHz
11,3	13.417 KHz

1. Report No.	2. Government Accession No.	3. Recipient's Catalog No.
NASA CR-3416		

4. Title and Subtitle	5. Report Date
INVESTIGATION OF THE EFFECTS OF INLET SHAPES ON FAN NOISE RADIATION	April 1981
	6. Performing Organization Code
7. Author(s)	8. Performing Organization Report No.
T. L. Clark, D. R. Slotboom, and P. G. Vaidya	
	10. Work Unit No.
9. Performing Organization Name and Address	
Boeing Commercial Airplane Company P.O. Box 3707 Seattle, Washington 98124	11. Contract or Grant No. NAS1-15394
	13. Type of Report and Period Covered Contractor Report
12. Sponsoring Agency Name and Address	
National Aeronautics and Space Administration Washington, D. C. 20546	14. Sponsoring Agency Code

15. Supplementary Notes

Langley Technical Monitor: Lorenzo R. Clark
Final Report

16. Abstract

It is known from model fan static tests that inlet shape has a significant effect on forward radiated fan tone noise directivities. This report describes the results of a study of this effect under experimentally simplified zero flow conditions.

Simulated fan tone noise was radiated to the far field through various shaped zero flow "inlets." Baseline data were collected for the simplest baffled and unbaffled straight pipe inlets. These data compared well with prediction. The more general inlet shapes tested were the conical, circular, and exponential surfaces of revolution and an asymmetric inlet achieved by cutting a straight pipe inlet at an acute angle. Approximate theories were developed for these general shapes and some comparisons with data are presented.

The conical and exponential shapes produced directivities that differed considerably from the baseline data while the circular shape produced directivities similar to the baseline data. The asymmetric inlet produced asymmetric directivities with significant reductions over the straight pipe data for some angles.

17. Key Words (Suggested by Author(s))	18. Distribution Statement
Radiation, Inlet Shape, Fan Noise, Directivity Effect	Unclassified - Unlimited Subject Category 71

19. Security Classif. (of this report)	20. Security Classif. (of this page)	21. No. of Pages	22. Price
Unclassified	Unclassified	47	A03

For Sale by the National Technical Information Service, Springfield, Virginia 22161